Congress of Neurological Surgeons

GUIDELINES

CONGRESS OF NEUROLOGICAL SURGEONS SYSTEMATIC REVIEW AND EVIDENCE-BASED GUIDELINE ON PREOPERATIVE IMAGING ASSESSMENT OF PATIENTS WITH SUSPECTED NONFUNCTIONING PITUITARY ADENOMAS

Sponsored by

Congress of Neurological Surgeons (CNS) and the AANS/CNS Tumor Section

Endorsed by

Joint Guidelines Committee of the American Association of Neurological Surgeons (AANS) and the Congress of Neurological Surgeons (CNS)

Clark C. Chen, MD, PhD[1], Bob S. Carter, MD, PhD[1], Renzhi Wang, MD[2], Kunal S. Patel, BA[1], Christopher Hess, MD, PhD[3], Mary E. Bodach, MLIS[4], Luis M. Tumialan MD[5], Nelson M. Oyesiku, MD, PhD[6], Chirag G. Patil, MD[7], Zachary Litvack, MD[8], Gabriel Zada, MD[9], Manish K. Aghi, MD, PhD[10]

[1] Center for Theoretical and Applied Neuro-Oncology, Division of Neurosurgery, University of California, San Diego, San Diego, California, USA
[2] Department of Neurosurgery, Peking Union Medical College Hospital, Beijing, China
[3] Department of Radiology and Biomedical Imaging, University of California, San Francisco, San Francisco, California, USA
[4] Guidelines Department, Congress of Neurological Surgeons, Schaumburg, Illinois, USA
[5] Barrow Neurological Institute, Phoenix, Arizona, USA
[6] Department of Neurosurgery, Emory University, Atlanta, Georgia, USA
[7] Department of Neurosurgery, Cedars-Sinai Medical Center, Los Angeles, California, USA
[8] Department of Neurosurgery, George Washington University, Washington, DC, USA
[9] Department of Neurological Surgery, University of Southern California, Los Angeles, California, USA
[10] Department of Neurosurgery, University of California, San Francisco, San Francisco, California, USA

Correspondence:

Clark Chen, MD, PhD
Center for Theoretical and Applied Neuro-Oncology
Moores Cancer Center
University of California, San Diego
3855 Health Science Drive #0987
La Jolla, CA 92093-0987
E-mail: clarkchen@ucsd.edu

ABSTRACT

Background: The authors reviewed published articles pertaining to the preoperative imaging evaluation of nonfunctioning pituitary adenomas (NFPAs) and formulated recommendations.

Methods: The MEDLINE database was queried for studies investigating imaging for the preoperative evaluation of pituitary adenomas.

Results: From an initial search of 5598 articles, 122 articles were evaluated in detail and included in this article. Based on analysis of these articles, the recommendations are as follows: 1) High resolution magnetic resonance imaging (Level II) is recommended as the standard for preoperative assessment of NFPAs, but may be supplemented with CT (Level III) and fluoroscopy (Level III). 2) Although there are promising results suggesting the utility of magnetic resonance spectroscopy, magnetic resonance perfusion, positron emission tomography, and single-photon emission computed tomography, there is insufficient evidence to make formal recommendations pertaining to their clinical applications.

Conclusions: The authors identified 122 articles that form the basis of recommendations for preoperative imaging evaluation of NFPAs. Preoperative imaging assessment of NFPAs requires a thoughtful integration of multiple imaging modalities and judicious clinical assessment.

RECOMMENDATIONS

Question

What imaging modality should be carried out in the preoperative diagnosis of NFPAs?

Target population

These recommendations apply to adults with imaging findings, signs, and symptoms suggestive of a nonfunctioning pituitary adenoma.

Recommendation

High-resolution MRI (Level II) is recommended as the standard but may be supplemented with CT (Level III).

Question

What imaging modalities can be used to preoperatively evaluate NFPA histology and characteristics?

Target population

These recommendations apply to adults with imaging findings, signs, and symptoms suggestive of a nonfunctioning pituitary adenoma.

Recommendation

While promising results are available pertaining to MR spectroscopy, MR perfusion, PET, and SPECT for preoperative assessment of NFPA histology and characteristics, there is insufficient evidence to make a formal recommendation for their use.

Question

What imaging modalities can be used to preoperatively evaluate cavernous sinus invasion?

Target population

These recommendations apply to adults with imaging findings, signs, and symptoms suggestive of a nonfunctioning pituitary adenoma.

Recommendation

While promising results are available pertaining to high-resolution MR and proton density imaging as tools of assessing cavernous sinus invasion, there is insufficient evidence to make a formal recommendation for their use.

Question

What imaging modality can be used to preoperatively evaluate tumor vascularity and hemorrhage?

Target population

These recommendations apply to adults with imaging findings, signs, and symptoms suggestive of a nonfunctioning pituitary adenoma.

Recommendation

While promising results are available pertaining to perfusion and gradient echo imaging as tools for assessing tumor vascularity and hemorrhage, there is insufficient evidence to make a formal recommendation for their use.

INTRODUCTION

Surgical management of nonfunctioning pituitary adenomas (NFPAs) is largely based on imaging evaluation in the context of clinical assessment. To date, information pertaining to the preoperative radiography of pituitary lesions is derived entirely from retrospective series, with little contribution from prospective studies or randomized control trials (RCTs). This review aims to summarize the key studies that impact the clinical utilization of neuroimaging in the preoperative management of NFPAs.

METHODOLOGY

Process Overview

The evidence-based clinical practice guideline task force members and the Tumor Section of the American Association of Neurological Surgeons (AANS) and the Congress of Neurological Surgeons (CNS) conducted a systematic review of the literature relevant to the management of nonfunctioning pituitary adenomas (NFPAs). Additional details of the systematic review are provided below and within the introduction and methodology chapter of the guideline.

Disclaimer of Liability

This clinical systematic review and evidence-based guideline was developed by a physician volunteer task force as an educational tool that reflects the current state of knowledge at the time of completion. The presentations are designed to provide an accurate review of the subject matter covered. This guideline is disseminated with the understanding that the recommendations by the authors and consultants who have collaborated in its development are not meant to replace the individualized care and treatment advice from a patient's physician(s). If medical advice or assistance is required, the services of a physician should be sought. The recommendations contained in this guideline may not be suitable for use in all circumstances. The choice to implement any particular recommendation contained in this guideline must be made by a managing physician in light of the situation in each particular patient and on the basis of existing resources.

Potential Conflicts of Interest

All NFPA Guideline Task Force members were required to disclose all potential conflicts of interest (COIs) prior to beginning work on the guideline, using the COI disclosure form of the AANS/CNS Joint Guidelines Committee. The CNS Guidelines Committee and Guideline Task Force Chair reviewed the disclosures and either approved or disapproved the nomination and participation on the task force. The CNS Guidelines Committee and Guideline Task Force Chair may approve nominations of Task Force Members with possible conflicts and restrict the writing, reviewing and/or voting privileges of that person to topics that are unrelated to the possible COIs.

Literature Search

The Task Force collaborated with a medical librarian to search for articles published from January 1, 1966, to October 1, 2014 in both PubMed and The Cochrane Central Register of Controlled Trials. Strategies for searching electronic databases were constructed by the guideline taskforce members and the medical librarian using previously published search strategies to identify relevant studies (Appendix A).[1-8]

RESULTS

Study Selection

An independent reviewer evaluated the initial 5598 citations using the criteria described above. Articles were excluded for the following reasons: 905 articles were not written in English, 82 articles involved only animal studies, 1810 articles were case reports, 1465 articles did not involve NFPAs, 998 articles did not involve imaging, 48 studies described postoperative assessment of NFPAs, and 55 studies described the use of intraoperative MRIs. After these exclusions, 235 articles were evaluated in detail for the purpose of this review. The same eligibility criteria were used for full-text screening of potentially relevant papers. Overall, 122 studies met the eligibility criteria for this systematic review, including 8 studies producing Class II data and 114 studies producing Class III data related to preoperative imaging for NFPAs. Figure 1 outlines the flow of studies through the review process.

Imaging Modalities

Computed Tomography (CT) Imaging

Prior to the advent of MR imaging, CT imaging[9-16] and CT cisternography[17,18] were used as feasible options for the diagnosis of sellar lesions, supported predominantly with Class III data (Table 1). However, the limited soft-tissue resolution of these modalities rendered limited information on NFPAs.[19,20] While MRI has emerged as the gold standard for preoperative imaging diagnosis of sellar/suprasellar lesions, some surgeons prefer to augment MRI with imaging information from thin-cut CT through the sellar/sphenoid region and/or CT angiogram for preoperative planning and intraoperative navigation.[21] There are 2 reasons underlying this preference, each supported by Class III data. First, the sphenoid septal anatomy is better visualized on high-resolution CT relative to the various MRI sequences.[22-28] Second, inherent magnetic field homogeneity within regions of air-bone density causes image distortion on MRI, rendering the geometric accuracy of the image tenuous.[29]

Newer modes of CT imaging are now used to provide more detailed imaging information of sellar/suprasellar lesions when MRI is not accessible or is contraindicated. Multidetector-row CT takes advantage of concurrent acquisition of multiple slices in various directions to provide higher resolution imaging. Images acquired through this modality were found to provide sufficient NFPA visualization in a study of 33 patients with Class III data (Table 1).[23] Dual-energy CT is another imaging technique that utilizes high-frequency cycling of high/low voltages to improve the quality of the CT images acquired. Class III data examining this technique suggests that the modality can provide information that discriminates between pituitary adenomas and meningiomas with a sensitivity of 90.9% and specificity of 100%.[30]

Magnetic Resonance (MR) Imaging

There is no class I data comparing the sensitivity and specificity of CT and MRI in terms of the detection and characterization of pituitary lesions (Table 1 and Table 2). However, the studies with Class II data that compare CT and MRI have shown that MRI can provide more detailed images of sellar/suprasellar lesions relative to CT.[31,32] This conclusion is supported by several studies with Class III data.[25,28,33-35] In this context, MRI has emerged as the gold standard. Typically, dedicated MR images spaced 1-2 mm apart are obtained through the sellar/suprasellar region for imaging assessment. The anterior lobe of the normal pituitary gland is iso-intense to the imaging appearance of the cerebral gray matter on all MR sequences. As this region is one of the circumventricular organs without an intact blood-brain barrier, gadolinium freely perfuses this region, and the region enhances within 30 minutes of infusion.[36]

Because the sizes of NFPAs that require surgical attention are relatively large, most MR sequences, scanners, and contrast doses yield comparable results, supported by Class II and III data, in terms of lesion identification (Table 2).[25,37-45] This is in stark contrast to microadenoma detection, in which protocols for contrast administration and MR parameters significantly impact the diagnostic yield.[46] Nevertheless, visualization of fine anatomic details surrounding the tumor, such as cavernous sinus wall involvement, cranial nerve visualization, or the presence of hemorrhage is influenced by the magnetic strength of the scanner (1.5T versus 3T) as well as the type of MR sequence utilized. Pertinent literature on these matters will be reviewed below.

1.5T vs 3T scanners

The field strength of the magnet used for MRI has progressively increased[47,48] since its initial introduction for clinical use in the 1980s. In principle, imaging at higher field strengths should afford increased spatial resolution and improved anatomic visualization. Previous studies producing type III data largely supports this thesis (Table 3).[49] One means to evaluate this concept is the determination of imaging evidence of cavernous sinus invasion. To this end, Wolfsberger et al compared the sensitivity and specificity of 1.5T and 3T MR imaging in terms of the integrity of the medial cavernous sinus border in 21 patients who underwent surgical resection of pituitary lesions (Class III data).[50] Intraoperative findings of medial sinus wall integrity were used as a gold standard, and the imaging interpretations were compared to this gold standard. The authors report that, relative to 1.5T imaging, the 3T imaging yielded superior sensitivity (67% versus 83%, respectively) and specificity (58% relative to 84%) in terms of correlation to surgical findings. The authors additionally report that 3T MRI afforded improved resolution of the intracavernous cranial nerve segments as well as improved differentiation of optochiasmatic structures from the sellar lesion.[50]

Magnetic susceptibility effects present a significant obstacle to high-field MRI around the sella and central skull base. Tissue interfaces, especially around air- and bone-containing structures, cause non-uniformity in the otherwise homogeneous main magnetic field within an MRI scanner. The severity of non-uniformity increases with the strength of the main magnetic field and gives rise to geometric distortion and signal loss around these tissue interfaces. These magnetic susceptibility effects also render normal fat-suppression techniques less effective, making it more difficult to assess involvement of the bony structures around the sella.

Because of the increased resolution provided by higher strength MRIs, subtle patient motion related to respiratory effort has also been shown to compromise image quality. In one study with Class III data, volumetric interpolated breath-hold examination (VIBE, see definition below) was shown to improve the diagnostic utility of MR imaging (Table 4).[51] The necessity of these techniques is likely increased with the use of higher-field-strength MRIs.

Specific MR Sequences

In addition to the conventional T1 and T2 weighted sequences, specific MR techniques are used to characterize pituitary tumors in the preoperative setting. In this section we will provide an overview of these sequences and their application pertaining to NFPAs. The specifics of the type of information provided by these MR sequences are reviewed in the tumor characteristics section.

Constructive Interference Steady State (CISS) techniques such as fast imaging employing steady-state acquisition (FIESTA) use flow-compensated, 2- or 3-dimensional gradient echo acquisition to obtain images with contrast that is proportional to the ratio of T2 relation time to T1 relaxation time. Characterized by high signal-to-noise and high spatial resolution, CISS permits exquisite MR cisternography in order to depict boundaries between CSF and soft tissues.[52] Class III data have shown that signal intensity on CISS sequences is associated with the firmness of NFPAs (Table 4).[53]

Dynamic imaging during the intravenous administration of gadolinium chelate show the differential enhancement of structures within and around the sella, thereby allowing the temporal separation of enhancement within the normal pituitary gland, NFPA tumor tissue and vascular structures such as the cavernous sinuses. Although most practices employ 2-dimensional techniques for dynamic MRI in the sella, volumetric gradient-echo techniques can be performed using breath-hold techniques such as the volumetric interpolated breath-hold examination (VIBE) sequence.[54] The inherent advantage of 3D acquisition over 2D techniques lies in the ability to distinguish smaller structures with greater accuracy. Class III data suggest that VIBE sequence may offer superior image resolution of NFPA invasion of the cavernous sinus (Table 4).[51]

Proton density weighted imaging is a standard MR technique designed to minimize the effects of longitudinal relaxation time and local magnetic field inhomogeneity (or T2*) to yield images dependent primarily on the density of protons in the imaging volume. Signal intensity with proton density imaging is proportional to the concentration of hydrogen atoms (especially water molecules) in tissue. Class III data has shown that proton density weighted MR imaging is highly sensitive and specific for predicting NFPA invasion of the cavernous sinus (Table 4).[55]

Periodically rotated overlapping parallel lines with enhanced reconstruction (PROPELLER) is a technique that samples the MRI data measurement space using a set of radially directed strips in a rotating fashion. The technique is designed to reduce the sensitivity of MR to various sources of image artifacts, including motion, field inhomogeneity, and eddy current effects.[56] Class III data suggests this sequence may help to discriminate NFPAs from other sellar/suprasellar pathologies (Table 4).[57]

MR perfusion imaging can be achieved by a number of different techniques, including dynamic susceptibility contrast (DSC) imaging[58] and arterial spin labeling (ASL).[59] DSC evaluates the change in signal on T2*-weighted sequences as gadolinium contrast flows through tissue to calculate blood volume and blood flow. ASL magnetically labels water molecules within a fixed volume of blood and then evaluates the transit of labeled molecules through perfused tissue. Class III data has shown MR perfusion may be used for discriminating NFPAs from other sellar/suprasellar pathologies[60] and from the normal pituitary (Table 4).[61] There is also Class III data suggesting that perfusion studies also provide information regarding vascularity of the NFPA.[62]

Diffusion weighted imaging (DWI) is an MR imaging technique that correlates the intensity of each voxel in the image space to the rate of water diffusion of that voxel. A Class II study suggests DWI-based sequences may be used for discriminating NFPAs from other sellar/suprasellar pathologies, and Class III studies have used this for assessing tumor firmness (Table 4).[57,63,64]

MR spectroscopy is a technique that allows for detection of specific metabolites related to normal cerebral physiology of the tumor proteome. MR spectroscopy may provide information that affords discrimination of NFPAs from other sellar/suprasellar pathologies, including craniopharyngiomas and hypothalamic hamartomas. However, MR spectroscopy is technically challenging within small volumes such as the sella and is very sensitive to magnetic susceptibility effects due to the surrounding bone.

Gradient-echo image is generated by a frequency-encoded gradient that is applied twice in succession and in opposite directions.[65] Clinically, it is highly sensitive for the detection of intracerebral hemorrhages by compounding the influence of blood products.[66] GE sequences have been applied for detection of hemorrhagic conversion of NFPAs (Class III data) (Table 4).[66]

Positron Emission Tomography (PET) Imaging

In general, the utility of PET imaging in the assessment of pituitary lesions is limited and is not routinely used in standard practice. On rare occasions, FDG PET diagnoses patients with incidental pituitary lesions. In a retrospective study with Class III data of 40967 FDG PET performed at a single center, 30 (0.073%) patients were diagnosed with pituitary incidentalomas (Table 5).[67]

Though rarely used clinically in the standard assessment of NFPAs, select studies have examined the sensitivity and specificity of PET imaging as a possible diagnostic test. In 3 independent case series with Class III data utilizing 18(F)-FDG PET, detection of pituitary adenomas can be achieved with a sensitivity of 94%-100% and a sensitivity of 88%-100% (Table 5).[68-70] In these studies, 18(F) FDG PET provided information allowing for discrimination of pituitary adenomas from other sellar pathology like craniopharyngiomas and meningiomas. Furthermore, Class III data suggest [11C]-L-deprenyl PET may facilitate discrimination of meningiomas from NFPAs.[71]

Single-Photon Emission Computed Tomography (SPECT) Imaging

Like PET, SPECT is not routinely used during standard preoperative assessment of NFPAs. Nevertheless, select patients may benefit from SPECT imaging. The uses of different compounds in SPECT have been evaluated. SPECT using iodinated dopamine D2 antagonist S(-) iodobenzamide (IBZM) or similar compounds demonstrated that D2 receptors in pituitary adenomas can be visualized using SPECT (Class III data) (Table 6).[72] Technetium-99m-hexakis-2-methyoxy-isobutyl-isonitrile SPECT can discriminate NFPAs from normal pituitary gland (Class III data).[73] ^{99m}Tc(V)-DMSA is actively taken up by NFPAs relative to other sellar/suprasellar lesions and has been shown with Class III data that it can be applied to differentiate NFPAs.[74,75] Use of radiolabeled somatostatin or dopamine can potentially differentiate hormone producing from nonfunctioning pituitary adenomas and identify patients who would benefit from pharmacotherapy, although the clinical feasibility of this is unclear (Class III data).[76-84] Similarly, while other radiopharmaceuticals have been shown to bind to NFPAs in studies with Class III data,[85,86] the diagnostic utility these finding remain unclear.

Preoperative Imaging Characterization of NFPAs

Use of Preoperative Imaging to Differentiate NFPAs from Other Pathologies

One of the most challenging aspects in preoperative assessment of NFPAs involves differentiation from the other lesions that occur in this region. Such discrimination affords neurosurgeons an opportunity to tailor the surgical approach for resection or use specific pharmacotherapy.

MR spectroscopy may be helpful in this regard. For instance, both hypothalamic hamartomas and gliomas exhibit decreased N-acetyl asparate (NAA).[87,88] However, hypothalamic hamartomas are characterized by increased myoinositol while hypothalamic gliomas show

increased choline accumulation.[88] Class III data found that pituitary adenomas, on the other hand, often show a choline peak (Table 7).[89] Craniopharyngiomas and germinomas both show dominant lipid peaks.[90-92] One study with Class III data demonstrated that the integration of spectroscopy data with conventional MRI sequences better enables preoperative assessment of sellar/suprasellar lesions.[93]

Other imaging techniques also contribute information that affords better preoperative assessment of NFPAs. One study compared MR perfusion images in 41 patients with sellar tumors to definitive tissue diagnosis and found higher cerebral blood volume values in meningiomas relative to NFPAs (Table 7).[60] In addition, [^{99m}Tc(V)-DMSA] demonstrates active uptake in NFPAs relative to other sellar/suprasellar lesions.[74,75]

Preoperative MR imaging appearances of pituitary adenomas have been associated with their hormone secretory status. One study with Class III data reported that the degree of enhancement on T1-weighted sequences correlate with the proportion of hormone-positive cells (Table 7).[94] Another study with Class III data reported that lowered T1 relaxation rate was associated with NFPAs relative to secreting adenomas.[95] Finally, there is a series of studies with Class III data demonstrating that increased tumor extension into adjacent anatomic compartments and cavernous sinus invasion are characteristics associated with NFPAs.[96-99]

The utility of PET and SPECT for discriminating NFPAs from hormone-secreting macroadenomas are reviewed under the sections on PET and SPECT imaging.

Studies with Class III evidence have shown that different histologic subtypes of NFPAs (null cell adenomas, silent corticotroph, or silent gonadotroph adenomas) are also associated with distinct MR appearances. Class III data suggests that multiple microcysts on T2W imaging, cavernous sinus invasion, lobulated appearance, and size >40 mm are associated with silent corticotroph adenomas (Table 7).[100,101] Furthermore, Class II data suggest biochemical properties of the tumors are associated with specific MR characteristics.[102]

Cavernous Sinus Wall Invasion

Assessment of NFPA invasion into the cavernous sinus can facilitate determination of surgical end-point and strategy (Table 8).[103] The most common MR sequences for evaluation of sinus invasion are thin-cut T1 and T2W studies, with intent for visualizing the medial wall of the cavernous sinus (Class III).[104,105] Recent studies suggest that proton density weighted or VIBE sequences may yield improved detection of cavernous sinus wall invasion.[51] However, no imaging techniques will perfectly predict NFPA sinus invasion because it is not always possible to directly visualize the medial cavernous sinus wall in patients afflicted with NFPAs.

To address this deficiency, various imaging parameters, supported by Class III, have been proposed as criteria for assessing cavernous sinus wall invasion (Table 8).[106,107] The Knosp criteria is a scale that classified NFPAs by the extent of parasellar extension relative to inter-carotid lines drawn through the intra-cavernous carotid on a coronal MRI.[108] High Knosp grades are associated with increased likelihood of sinus invasion. Variations of this scale, evaluated with Class III data, involve quantitating the extent that the tumor encases the intra-cavernous carotid[109-111] or involvement of the different cavernous sinus compartments.[112-114]

Higher degree of encasement is associated with higher likelihood of sinus invasion. Detection of normal pituitary between NFPA and the cavernous sinus, sometimes called "rim sign" or "peri-arterial enhancement," can be helpful to exclude sinus invasion.[40,115] Asymmetric dural enhancement of tentorium along the posterior portion of the cavernous sinus is associated with increased likelihood of sinus invasion and thought to be related to venous congestion secondary to tumor mass (type III).[116,117]

Additionally, functional imaging through SPECT and PET facilitate the discrimination of pituitary adenomas varying in invasive tendencies. Retrospective series with Class III data report that the uptake of technetium-99m sestamibi (SPECT) or 201Tl chloride (SPECT) is higher in invasive NFPAs (Table 8).[101,118,119]

Vascularity and Hemorrhage

Preoperative assessment of tumor enhancement patterns and vascularity may facilitate strategies for management of intra- and postoperative tumor hemorrhage.[120-123] These studies have been supported by Class III data (Table 9). Retrospective series suggest that ASL and DSC measurements correlate with tumor vascularity. Higher ASL blood flow values correlated with intraoperative findings of NFPA vascularity and risk of postoperative hemorrhage.[62] Similarly, DSC indicative of increased blood flow correlated with histologic evidence of vascularity for NFPAs. While these initial studies report promising results, the use of these techniques in preoperative imaging assessment of NFPAs remains investigational and have not been incorporated into standard practice.

Detection of intra-tumoral hemorrhage in NFPAs is also of critical importance in terms of clinical management. These events in the context of clinical deterioration warrant emergent neurosurgical intervention. Most acute hemorrhages appear T1 hypo-intense and T2 hyper-intense (Class III data) (Table 9).[124,125] Class III data suggest T2-weighted gradient-echo (GE) imaging can be used to further enhance the sensitivity of hemorrhage detection.[66,126] Lack of a strong choline peak on MR-spectroscopy was also associated with hemorrhage in NFPAs.[89]

Firmness of the Tumor Mass

Firm, fibrous tumors may be more difficult to manipulate intraoperatively.[127] Preoperative assessment may allow for application of different surgical strategies. Various MRI sequences with both Class II and III data have been used to evaluate the tissue quality of pituitary adenomas, using intraoperative findings as the gold standard (Table 10).[53,64,128,129] Retrospective series with Class III data demonstrate association between MR findings of homogenous intensity on T1W, T2W, and contrast enhancement studies with fibrous NFPAs.[53,129,130] While several studies have investigated the correlation between DWI findings and the firmness of NFPAs, these studies have yielded conflicting results. Of the 4 published studies, 2 studies with Class III data found no correlation,[63,64] 1 study with Class III data showed positive correlation,[131] and another with Class III data showed negative correlation.[132]

Pituitary Anatomy

Preoperative assessment of NFPAs involves visualization of the NFPA relative to pertinent sellar anatomy, including visualization of the normal pituitary gland, the pituitary stalk, the optic apparatus, and their relation to one another.

Because the pituitary gland is a circumventricular organ without an intact blood-brain barrier, the normal pituitary tissue typically exhibits higher intensity on contrast-enhanced T1W scans relative to NFPAs.[133] The normal pituitary gland is most often displaced superiorly and posteriorly by NFPAs.[133,134] Displacement of normal pituitary in other directions can suggest other pathology.[133,134]

The normal pituitary stalk is of relatively low intensity but can be bright when compressed by NFPAs and other sellar/suprasellar lesions (Class III data) (Table 11).[135] However, preoperative imaging findings of stalk compression/deviation or bright stalk are not always associated with elevated prolactin class expected of stalk effect (Class III data).[136] Nevertheless, there is an association between the imaging finding of "bright stalk" and NFPA size. One study with Class III data found that ectopic location of the bright spot is correlated with tumors larger than 20 mm.[137] Another study with Class III data showed that a posteriorly displaced "bright stalk" is associated with higher tumor volume ($P < .001$).[138] The shape of the NFPA can also be inferred by the location of the "bright stalk." "Bright stalk" found above the diaphragm was associated with an hourglass-shaped adenoma, whereas those found in the sella were associated with a barrel-shaped adenoma (Class III data).[139]

The relationship between the tumor and the optic apparatus is typically studied using thin-cut T2W images (Class III data) (Table 11).[140,141] While in most cases the optic chiasm is superior to the tumor, it can be found both anteriorly and posteriorly,[140] and detection of this may adjust surgical approach. Visual field loss is significantly correlated with the height of the chiasm and the tumor (Class III data)[142] as well as optic nerve hyperintensity on T2W images (Class II data),[143] but not with optic tract edema (Class III data).[144]

CONCLUSION

A wide range of anatomic and functional imaging modalities is currently available for preoperative assessment of NFPAs. Understanding the benefits and limitations of these modalities should afford opportunities for judicious clinical application, with the goal of optimizing patient care. Overcoming the limitations of current imaging tools will require thoughtful integration of technologic development and clinical validation.

Disclosure of Funding

These evidence-based clinical practice guidelines were funded exclusively by the CNS and the Tumor Section of the CNS and the AANS, which received no funding from outside commercial sources to support the development of this document.

Acknowledgments

The authors acknowledge the CNS Guidelines Committee for their contributions throughout the development of the guideline, the AANS/CNS Joint Guidelines Committee for their review, comments, and suggestions throughout peer review, and Pamela Shaw, MSLIS, MS, for assistance with the literature searches. The authors also acknowledge the following individual peer reviewers for their contributions: Sepideh Amin-Hanjani, MD, Kathryn Holloway, MD,

Odette Harris, MD, Brad Zacharia, MD, Daniel Hoh, MD, Isabelle Germano, MD, Martina Stippler, MD, Kimon Bekelis, MD, Christopher Winfree, MD, and William Mack, MD. Lastly, and most significantly, the authors would like to acknowledge Edward Laws, MD, for serving as an advisor on this nonfunctioning adenoma guidelines project and providing comprehensive critical appraisal.

Disclosures

The authors have no personal, financial, or institutional interest in any of the drugs, materials, or devices described in this article.

REFERENCES

1. Kastner M, Wilczynski NL, Walker-Dilks C, McKibbon KA, Haynes B. Age-specific search strategies for Medline. *J. Med. Internet Res.* 2006;8(4):e25.

2. Haynes RB, McKibbon KA, Wilczynski NL, Walter SD, Werre SR, Hedges T. Optimal search strategies for retrieving scientifically strong studies of treatment from Medline: analytical survey. *BMJ.* 2005;330(7501):1179.

3. Montori VM, Wilczynski NL, Morgan D, Haynes RB, Hedges T. Optimal search strategies for retrieving systematic reviews from Medline: analytical survey. *BMJ.* 2005;330(7482):68.

4. Wong SS, Wilczynski NL, Haynes RB. Comparison of top-performing search strategies for detecting clinically sound treatment studies and systematic reviews in MEDLINE and EMBASE. *Journal of the Medical Library Association : JMLA.* 2006;94(4):451-455.

5. Zhang L, Ajiferuke I, Sampson M. Optimizing search strategies to identify randomized controlled trials in MEDLINE. *BMC Med. Res. Methodol.* 2006;6:23.

6. Topfer LA, Parada A, Menon D, Noorani H, Perras C, Serra-Prat M. Comparison of literature searches on quality and costs for health technology assessment using the MEDLINE and EMBASE databases. *Int. J. Technol. Assess. Health Care.* 1999;15(2):297-303.

7. Wilczynski NL, Haynes RB. Developing optimal search strategies for detecting clinically sound prognostic studies in MEDLINE: an analytic survey. *BMC Med.* 2004;2:23.

8. Wilczynski NL, Haynes RB, Hedges T. EMBASE search strategies achieved high sensitivity and specificity for retrieving methodologically sound systematic reviews. *J. Clin. Epidemiol.* 2007;60(1):29-33.

9. Clark WC, Acker JD, Robertson JH, Eggers F, Muhlbauer MS. Reformatted sagittal images in the differential diagnosis of meningiomas and pituitary adenomas with suprasellar extension. *Neurosurgery.* 1986;18(5):555-558.

10. Chen XR, Shen TZ, Chen GB, Tang SS. Computed tomography in the diagnosis of pituitary adenoma. *Comput. Radiol.* 1982;6(3):125-135.

11. Daniels DL, Williams AL, Thornton RS, Meyer GA, Cusick JF, Haughton VM. Differential diagnosis of intrasellar tumors by computed tomography. *Radiology.* 1981;141(3):697-701.

12. Robertson HJ, Rose A, Ehmi B, England G, Meriweather R. Trends in the radiological study of pituitary adenoma. *Neuroradiology.* 1981;21(2):75-78.

13. Gardeur D, Naidich TP, Metzger J. CT analysis of intrasellar pituitary adenomas with emphasis on patterns of contrast enhancement. *Neuroradiology.* 1981;20(5):241-247.

14. Macpherson P, Anderson DE. Radiological differentiation of intrasellar aneurysms from pituitary tumours. *Neuroradiology.* 1981;21(4):177-183.

15. Hatam A, Bergström M, Greitz T. Diagnosis of sellar and parasellar lesions by computed tomography. *Neuroradiology*. 1979;18(5):249-258.

16. Gyldensted C, Karle A. Computed tomography of intra- and juxtasellar lesions. A radiological study of 108 cases. *Neuroradiology*. 1977;14(1):5-13.

17. Numaguchi Y, Kishikawa T, Ikeda J, et al. Neuroradiological manifestations of suprasellar pituitary adenomas, meningiomas and craniopharyngiomas. *Neuroradiology*. 1981;21(2):67-74.

18. Hall K, McAllister VL. Metrizamide cisternography in pituitary and juxtapituitary lesions. *Radiology*. 1980;134(1):101-108.

19. Davis PC, Hoffman JC, Tindall GT, Braun IF. CT-surgical correlation in pituitary adenomas: evaluation in 113 patients. *AJNR Am. J. Neuroradiol.* 1985;6(5):711-716.

20. Sakoda K, Mukada K, Yonezawa M, et al. CT scan of pituitary adenomas. *Neuroradiology*. 1981;20(5):249-253.

21. Swearingen B. Update on pituitary surgery. *J. Clin. Endocrinol. Metab*. 2012;97(4):1073-1081.

22. Hamid O, El Fiky L, Hassan O, Kotb A, El Fiky S. Anatomic Variations of the Sphenoid Sinus and Their Impact on Trans-sphenoid Pituitary Surgery. *Skull Base*. 2008;18(1):9-15.

23. Miki Y, Kanagaki M, Takahashi JA, et al. Evaluation of pituitary macroadenomas with multidetector-row CT (MDCT): comparison with MR imaging. *Neuroradiology*. 2007;49(4):327-333.

24. Abe T, Izumiyama H, Fujisawa I. Evaluation of pituitary adenomas by multidirectional multislice dynamic CT. *Acta Radiol.* 2002;43(6):556-559.

25. Lundin P, Bergström K, Thuomas KA, Lundberg PO, Muhr C. Comparison of MR imaging and CT in pituitary macroadenomas. *Acta Radiol.* 1991;32(3):189-196.

26. Wu W, Thuomas KA. Pituitary microadenoma. MR appearance and correlation with CT. *Acta Radiol.* 1995;36(5):529-535.

27. Johnson MR, Hoare RD, Cox T, et al. The evaluation of patients with a suspected pituitary microadenoma: computer tomography compared to magnetic resonance imaging. *Clin. Endocrinol. (Oxf.).* 1992;36(4):335-338.

28. Kaufman B, Kaufman BA, Arafah BM, Roessmann U, Selman WR. Large pituitary gland adenomas evaluated with magnetic resonance imaging. *Neurosurgery*. 1987;21(4):540-546.

29. Chen C, Chapman P, H K, JS L. Neuroimaging in radiosurgery treatment planning and follow-up evaluation. In: Chin L, Regine W, eds. *Principles and practice of stereotactic radiosurgery*. New York: Springer; 2008:9-23.

30. Wu LM, Li YL, Yin YH, et al. Usefulness of dual-energy computed tomography imaging in the differential diagnosis of sellar meningiomas and pituitary adenomas: preliminary report. *PLoS One*. 2014;9(3):e90658.

31. Guy RL, Benn JJ, Ayers AB, et al. A comparison of CT and MRI in the assessment of the pituitary and parasellar region. *Clin. Radiol.* 1991;43(3):156-161.

32. Davis PC, Hoffman JC, Spencer T, Tindall GT, Braun IF. MR imaging of pituitary adenoma: CT, clinical, and surgical correlation. *AJR Am. J. Roentgenol.* 1987;148(4):797-802.

33. Lee BC, Deck MD. Sellar and juxtasellar lesion detection with MR. *Radiology.* 1985;157(1):143-147.

34. Karnaze MG, Sartor K, Winthrop JD, Gado MH, Hodges FJ. Suprasellar lesions: evaluation with MR imaging. *Radiology.* 1986;161(1):77-82.

35. Mikhael MA, Ciric IS. MR imaging of pituitary tumors before and after surgical and/or medical treatment. *J. Comput. Assist. Tomogr.* 1988;12(3):441-445.

36. Castillo M. Pituitary gland: development, normal appearances, and magnetic resonance imaging protocols. *Top. Magn. Reson. Imaging.* 2005;16(4):259-268.

37. Gutenberg A, Larsen J, Lupi I, Rohde V, Caturegli P. A radiologic score to distinguish autoimmune hypophysitis from nonsecreting pituitary adenoma preoperatively. *AJNR Am. J. Neuroradiol.* 2009;30(9):1766-1772.

38. Kucharczyk W, Davis DO, Kelly WM, Sze G, Norman D, Newton TH. Pituitary adenomas: high-resolution MR imaging at 1.5 T. *Radiology.* 1986;161(3):761-765.

39. Steiner E, Imhof H, Knosp E. Gd-DTPA enhanced high resolution MR imaging of pituitary adenomas. *Radiographics.* 1989;9(4):587-598.

40. Steiner E, Math G, Knosp E, Mostbeck G, Kramer J, Herold CJ. MR-appearance of the pituitary gland before and after resection of pituitary macroadenomas. *Clin. Radiol.* 1994;49(8):524-530.

41. Hayashi S, Ito K, Shimada M, et al. Dynamic MRI with slow injection of contrast material for the diagnosis of pituitary adenoma. *Radiat. Med.* 1995;13(4):167-170.

42. Hald JK, Skalpe IO, Bakke SJ, Nakstad PH. MR imaging of pituitary region lesions with gadodiamide injection. *Acta Radiol.* 1994;35(1):65-69.

43. Davis PC, Gokhale KA, Joseph GJ, et al. Pituitary adenoma: correlation of half-dose gadolinium-enhanced MR imaging with surgical findings in 26 patients. *Radiology.* 1991;180(3):779-784.

44. Cury ML, Fernandes JC, Machado HR, Elias LL, Moreira AC, Castro M. Non-functioning pituitary adenomas: clinical feature, laboratorial and imaging assessment, therapeutic management and outcome. *Arq. Bras. Endocrinol. Metabol.* 2009;53(1):31-39.

45. Lundin P, Bergstrom K. Gd-DTPA-enhanced MR imaging of pituitary macroadenomas. *Acta Radiol.* 1992;33(4):323-332.

46. Chowdhury IN, Sinaii N, Oldfield EH, Patronas N, Nieman LK. A change in pituitary magnetic resonance imaging protocol detects ACTH-secreting tumours in patients with previously negative results. *Clin. Endocrinol. (Oxf.).* 2010;72(4):502-506.

47. Sekiya T, Fukuda Y, Kobayashi H, Hata Y, Tada S. Magnetic resonance imaging of the normal pituitary gland and pituitary adenoma: preliminary experience with a resistive magnet. *Radiat. Med.* 1985;3(3):131-136.

48. Oot R, New PF, Buonanno FS, et al. MR imaging of pituitary adenomas using a prototype resistive magnet: preliminary assessment. *AJNR Am. J. Neuroradiol.* 1984;5(2):131-137.

49. Pinker K, Ba-Ssalamah A, Wolfsberger S, Mlynarik V, Knosp E, Trattnig S. The value of high-field MRI (3T) in the assessment of sellar lesions. *Eur. J. Radiol.* 2005;54(3):327-334.

50. Wolfsberger S, Ba-Ssalamah A, Pinker K, et al. Application of three-tesla magnetic resonance imaging for diagnosis and surgery of sellar lesions. *J. Neurosurg.* 2004;100(2):278-286.

51. Davis MA, Castillo M. Evaluation of the pituitary gland using magnetic resonance imaging: T1-weighted vs. VIBE imaging. *Neuroradiol. J.* 2013;26(3):297-300.

52. Nitz WR. Fast and ultrafast non-echo-planar MR imaging techniques. *Eur. Radiol.* 2002;12(12):2866-2882.

53. Yamamoto J, Kakeda S, Shimajiri S, et al. Tumor consistency of pituitary macroadenomas: predictive analysis on the basis of imaging features with contrast-enhanced 3D FIESTA at 3T. *AJNR Am. J. Neuroradiol.* 2014;35(2):297-303.

54. Rofsky NM, Lee VS, Laub G, et al. Abdominal MR imaging with a volumetric interpolated breath-hold examination. *Radiology.* 1999;212(3):876-884.

55. Cao L, Chen H, Hong J, Ma M, Zhong Q, Wang S. Magnetic resonance imaging appearance of the medial wall of the cavernous sinus for the assessment of cavernous sinus invasion by pituitary adenomas. *J. Neuroradiol.* 2013;40(4):245-251.

56. Pipe JG, Farthing VG, Forbes KP. Multishot diffusion-weighted FSE using PROPELLER MRI. *Magn. Reson. Med.* 2002;47(1):42-52.

57. Mahmoud OM, Tominaga A, Amatya VJ, et al. Role of PROPELLER diffusion weighted imaging and apparent diffusion coefficient in the diagnosis of sellar and parasellar lesions. *Eur. J. Radiol.* 2010;74(3):420-427.

58. Belliveau JW, Rosen BR, Kantor HL, et al. Functional cerebral imaging by susceptibility-contrast NMR. *Magn. Reson. Med.* 1990;14(3):538-546.

59. Detre JA, Zhang W, Roberts DA, et al. Tissue specific perfusion imaging using arterial spin labeling. *NMR Biomed.* 1994;7(1-2):75-82.

60. Bladowska J, Zimny A, Guziński M, et al. Usefulness of perfusion weighted magnetic resonance imaging with signal-intensity curves analysis in the differential diagnosis of sellar and parasellar tumors: preliminary report. *Eur. J. Radiol.* 2013;82(8):1292-1298.

61. Manfré L, Midiri M, Rosato F, Janni A, Lagalla R. Perfusion MRI in normal and abnormal pituitary gland. A preliminary study. *Clin. Imaging.* 1997;21(5):311-318.

62. Sakai N, Koizumi S, Yamashita S, et al. Arterial spin-labeled perfusion imaging reflects vascular density in nonfunctioning pituitary macroadenomas. *AJNR Am. J. Neuroradiol.* 2013;34(11):2139-2143.

63. Mahmoud OM, Tominaga A, Amatya VJ, et al. Role of PROPELLER diffusion-weighted imaging and apparent diffusion coefficient in the evaluation of pituitary adenomas. *Eur. J. Radiol.* 2011;80(2):412-417.

64. Suzuki C, Maeda M, Hori K, et al. Apparent diffusion coefficient of pituitary macroadenoma evaluated with line-scan diffusion-weighted imaging. *J. Neuroradiol.* 2007;34(4):228-235.

65. Steinberg PM, Ross JS, Modic MT, Tkach J, Masaryk TJ, Haacke EM. The value of fast gradient-echo MR sequences in the evaluation of brain disease. *AJNR Am. J. Neuroradiol.* 1990;11(1):59-67.

66. Unger EC, Cohen MS, Brown TR. Gradient-echo imaging of hemorrhage at 1.5 Tesla. *Magn. Reson. Imaging.* 1989;7(2):163-172.

67. Jeong SY, Lee SW, Lee HJ, et al. Incidental pituitary uptake on whole-body 18F-FDG PET/CT: a multicentre study. *Eur. J. Nucl. Med. Mol. Imaging.* 2010;37(12):2334-2343.

68. Hyun SH, Choi JY, Lee KH, Choe YS, Kim BT. Incidental focal 18F-FDG uptake in the pituitary gland: clinical significance and differential diagnostic criteria. *J. Nucl. Med.* 2011;52(4):547-550.

69. Seok H, Lee EY, Choe EY, et al. Analysis of 18F-fluorodeoxyglucose positron emission tomography findings in patients with pituitary lesions. *Korean J. Intern. Med.* 2013;28(1):81-88.

70. Lucignani G, Losa M, Moresco RM, et al. Differentiation of clinically non-functioning pituitary adenomas from meningiomas and craniopharyngiomas by positron emission tomography with [18F]fluoro-ethyl-spiperone. *Eur. J. Nucl. Med.* 1997;24(9):1149-1155.

71. Bergström M, Muhr C, Lundberg PO, Långström B. PET as a tool in the clinical evaluation of pituitary adenomas. *J. Nucl. Med.* 1991;32(4):610-615.

72. de Herder WW, Reijs AE, de Swart J, et al. Comparison of iodine-123 epidepride and iodine-123 IBZM for dopamine D2 receptor imaging in clinically non-functioning pituitary macroadenomas and macroprolactinomas. *Eur. J. Nucl. Med.* 1999;26(1):46-50.

73. Kojima T, Mizumura S, Kumita SI, Kumazaki T, Teramoto A. Is technetium-99m-MIBI taken up by the normal pituitary gland? A comparison of normal pituitary glands and pituitary adenomas. *Ann. Nucl. Med.* 2001;15(4):321-327.

74. Yamamura K, Suzuki S, Yamamoto I. Differentiation of pituitary adenomas from other sellar and parasellar tumors by 99mTc(V)-DMSA scintigraphy. *Neurol. Med. Chir. (Tokyo).* 2003;43(4):181-186; discussion 187.

75. Lastoria S, Colao A, Vergara E, et al. Technetium-99m pentavalent dimercaptosuccinic acid imaging in patients with pituitary adenomas. *Eur. J. Endocrinol.* 1995;133(1):38-47.

76. Colao A, Lastoria S, Ferone D, et al. The pituitary uptake of (111)In-DTPA-D-Phe1-octreotide in the normal pituitary and in pituitary adenomas. *J. Endocrinol. Invest.* 1999;22(3):176-183.

77. Oppizzi G, Cozzi R, Dallabonzana D, et al. Scintigraphic imaging of pituitary adenomas: an in vivo evaluation of somatostatin receptors. *J. Endocrinol. Invest.* 1998;21(8):512-519.

78. Broson-Chazot F, Houzard C, Ajzenberg C, et al. Somatostatin receptor imaging in somatotroph and non-functioning pituitary adenomas: correlation with hormonal and visual responses to octreotide. *Clin. Endocrinol. (Oxf.).* 1997;47(5):589-598.

79. Rieger A, Rainov NG, Elfrich C, et al. Somatostatin receptor scintigraphy in patients with pituitary adenoma. *Neurosurg. Rev.* 1997;20(1):7-12.

80. de Herder WW, Reijs AE, Kwekkeboom DJ, et al. In vivo imaging of pituitary tumours using a radiolabelled dopamine D2 receptor radioligand. *Clin. Endocrinol. (Oxf.).* 1996;45(6):755-767.

81. Luyken C, Hildebrandt G, Krisch B, Scheidhauer K, Klug N. Clinical relevance of somatostatin receptor scintigraphy in patients with skull base tumours. *Acta Neurochir. Suppl.* 1996;65:102-104.

82. Tumiati MN, Facchi E, Gatti C, Bossi A, Longari V. Scintigraphic assessment of pituitary adenomas and several diseases by indium-111-pentetreotide. *Q. J. Nucl. Med.* 1995;39(4 Suppl 1):98-100.

83. Boni G, Ferdeghini M, Bellina CR, et al. [111In-DTPA-D-Phe]-octreotide scintigraphy in functioning and non-functioning pituitary adenomas. *Q. J. Nucl. Med.* 1995;39(4 Suppl 1):90-93.

84. Duet M, Mundler O, Ajzenberg C, et al. Somatostatin receptor imaging in non-functioning pituitary adenomas: value of an uptake index. *Eur. J. Nucl. Med.* 1994;21(7):647-650.

85. Colombo P, Siccardi AG, Paganelli G, et al. Three-step immunoscintigraphy with anti-chromogranin A monoclonal antibody in tumours of the pituitary region. *Eur. J. Endocrinol.* 1996;135(2):216-221.

86. Kurtulmus N, Turkmen C, Yarman S, Tokmak H, Mudun A. The value of Tc-99m tetrofosmin in the imaging of pituitary adenomas. *J. Endocrinol. Invest.* 2007;30(2):86-90.

87. Amstutz DR, Coons SW, Kerrigan JF, Rekate HL, Heiserman JE. Hypothalamic hamartomas: Correlation of MR imaging and spectroscopic findings with tumor glial content. *AJNR Am. J. Neuroradiol.* 2006;27(4):794-798.

88. Freeman JL, Coleman LT, Wellard RM, et al. MR imaging and spectroscopic study of epileptogenic hypothalamic hamartomas: analysis of 72 cases. *AJNR Am. J. Neuroradiol.* 2004;25(3):450-462.

89. Stadlbauer A, Buchfelder M, Nimsky C, et al. Proton magnetic resonance spectroscopy in pituitary macroadenomas: preliminary results. *J. Neurosurg.* 2008;109(2):306-312.

90. Kendi TK, Caglar S, Huvaj S, Bademci G, Kendi M, Alparslan S. Suprasellar germ cell tumor with subarachnoid seeding MRI and MR spectroscopy findings. *Clin. Imaging.* 2004;28(6):404-407.

91. Sutton LN, Wang ZJ, Wehrli SL, et al. Proton spectroscopy of suprasellar tumors in pediatric patients. *Neurosurgery.* 1997;41(2):388-394; discussion 394-385.

92. Sener RN. Proton MR spectroscopy of craniopharyngiomas. *Comput. Med. Imaging Graph.* 2001;25(5):417-422.

93. Faghih Jouibari M, Ghodsi SM, Akhlaghpoor S, et al. Complementary effect of H MRS in diagnosis of suprasellar tumors. *Clin. Imaging.* 2012;36(6):810-815.

94. Kobayashi S, Ikeda H, Yoshimoto T. A clinical and histopathological study of factors affecting MRI signal intensities of pituitary adenomas. *Neuroradiology.* 1994;36(4):298-302.

95. Spiller M, Childress SM, Koenig SH, et al. Secretory and nonsecretory pituitary adenomas are distinguishable by 1/T1 magnetic relaxation rates at very low magnetic fields in vitro. *Invest. Radiol.* 1997;32(6):320-329.

96. Zada G, Lin N, Laws ER, Jr. Patterns of extrasellar extension in growth hormone-secreting and nonfunctional pituitary macroadenomas. *Neurosurg. Focus.* 2010;29(4):E4.

97. Luo CB, Teng MM, Chen SS, et al. Imaging of invasiveness of pituitary adenomas. *Kaohsiung J. Med. Sci.* 2000;16(1):26-31.

98. Lundin P, Nyman R, Burman P, Lundberg PO, Muhr C. MRI of pituitary macroadenomas with reference to hormonal activity. *Neuroradiology.* 1992;34(1):43-51.

99. Chang CY, Luo CB, Teng MM, et al. Computed tomography and magnetic resonance imaging characteristics of giant pituitary adenomas. *J. Formos. Med. Assoc.* 2000;99(11):833-838.

100. Cazabat L, Dupuy M, Boulin A, et al. Silent, but not unseen: multimicrocystic aspect on T2-weighted MRI in silent corticotroph adenomas. *Clin. Endocrinol. (Oxf.).* 2014;81(4):566-572.

101. Nishioka H, Inoshita N, Sano T, Fukuhara N, Yamada S. Correlation between histological subtypes and MRI findings in clinically nonfunctioning pituitary adenomas. *Endocr. Pathol.* 2012;23(3):151-156.

102. Pan LX, Chen ZP, Liu YS, Zhao JH. Magnetic resonance imaging and biological markers in pituitary adenomas with invasion of the cavernous sinus space. *J. Neurooncol.* 2005;74(1):71-76.

103. Connor SE, Wilson F, Hogarth K. Magnetic resonance imaging criteria to predict complete excision of parasellar pituitary macroadenoma on postoperative imaging. *J Neurol Surg B Skull Base.* 2014;75(1):41-46.

104. Daniels DL, Czervionke LF, Bonneville JF, et al. MR imaging of the cavernous sinus: value of spin echo and gradient recalled echo images. *AJR Am. J. Roentgenol.* 1988;151(5):1009-1014.

105. Ahmadi J, North CM, Segall HD, Zee CS, Weiss MH. Cavernous sinus invasion by pituitary adenomas. *AJR Am. J. Roentgenol.* 1986;146(2):257-262.

106. Cukiert A, Andrioli M, Goldman J, et al. Cavernous sinus invasion by pituitary macroadenomas. Neuroradiological, clinical and surgical correlation. *Arq. Neuropsiquiatr.* 1998;56(1):107-110.

107. Knosp E, Kitz K, Steiner E, Matula C. Pituitary adenomas with parasellar invasion. *Acta Neurochir. Suppl. (Wien.).* 1991;53:65-71.

108. Knosp E, Steiner E, Kitz K, Matula C. Pituitary adenomas with invasion of the cavernous sinus space: a magnetic resonance imaging classification compared with surgical findings. *Neurosurgery.* 1993;33(4):610-617; discussion 617-618.

109. Scotti G, Yu CY, Dillon WP, et al. MR imaging of cavernous sinus involvement by pituitary adenomas. *AJR Am. J. Roentgenol.* 1988;151(4):799-806.

110. Sol YL, Lee SK, Choi HS, Lee YH, Kim J, Kim SH. Evaluation of MRI criteria for cavernous sinus invasion in pituitary macroadenoma. *J. Neuroimaging.* 2014;24(5):498-503.

111. Komiyama M, Hakuba A, Yasui T, et al. Magnetic resonance imaging of intracavernous pathology. *Neurol. Med. Chir. (Tokyo).* 1989;29(7):573-578.

112. Vieira JO, Cukiert A, Liberman B. Evaluation of magnetic resonance imaging criteria for cavernous sinus invasion in patients with pituitary adenomas: logistic regression analysis and correlation with surgical findings. *Surg. Neurol.* 2006;65(2):130-135; discussion 135.

113. Vieira JO, Cukiert A, Liberman B. Magnetic resonance imaging of cavernous sinus invasion by pituitary adenoma diagnostic criteria and surgical findings. *Arq. Neuropsiquiatr.* 2004;62(2B):437-443.

114. Cottier JP, Destrieux C, Brunereau L, et al. Cavernous sinus invasion by pituitary adenoma: MR imaging. *Radiology.* 2000;215(2):463-469.

115. Daita G, Yonemasu Y, Nakai H, Takei H, Ogawa K. Cavernous sinus invasion by pituitary adenomas--relationship between magnetic resonance imaging findings and histologically verified dural invasion. *Neurol. Med. Chir. (Tokyo).* 1995;35(1):17-21.

116. Nakasu Y, Nakasu S, Ito R, Mitsuya K, Fujimoto O, Saito A. Tentorial enhancement on MR images is a sign of cavernous sinus involvement in patients with sellar tumors. *AJNR Am. J. Neuroradiol.* 2001;22(8):1528-1533.

117. Cattin F, Bonneville F, Andréa I, Barrali E, Bonneville JF. Dural enhancement in pituitary macroadenomas. *Neuroradiology.* 2000;42(7):505-508.

118. Kunishio K, Okada M, Matsumoto Y, Nagao S, Nishiyama Y. Technetium-99m sestamibi single photon emission computed tomography findings correlated with P-glycoprotein expression in pituitary adenoma. *J. Med. Invest.* 2006;53(3-4):285-291.

119. Nakano T, Asano K, Tanaka M, Takahashi T, Miura H, Suzuki S. Use of 201Tl SPECT for evaluation of biologic behavior in pituitary adenomas. *J. Nucl. Med.* 2001;42(4):575-578.

120. Di Ieva A, Grizzi F, Ceva-Grimaldi G, et al. Fractal dimension as a quantitator of the microvasculature of normal and adenomatous pituitary tissue. *J. Anat.* 2007;211(5):673-680.

121. Finelli DA, Kaufman B. Varied microcirculation of pituitary adenomas at rapid, dynamic, contrast-enhanced MR imaging. *Radiology.* 1993;189(1):205-210.

122. Nägele T, Petersen D, Klose U, et al. Dynamic contrast enhancement of intracranial tumors with snapshot-FLASH MR imaging. *AJNR Am. J. Neuroradiol.* 1993;14(1):89-98.

123. Yuh WT, Fisher DJ, Nguyen HD, et al. Sequential MR enhancement pattern in normal pituitary gland and in pituitary adenoma. *AJNR Am. J. Neuroradiol.* 1994;15(1):101-108.

124. Kurihara N, Takahashi S, Higano S, et al. Hemorrhage in pituitary adenoma: correlation of MR imaging with operative findings. *Eur. Radiol.* 1998;8(6):971-976.

125. Lazaro CM, Guo WY, Sami M, et al. Haemorrhagic pituitary tumours. *Neuroradiology.* 1994;36(2):111-114.

126. Tosaka M, Sato N, Hirato J, et al. Assessment of hemorrhage in pituitary macroadenoma by T2*-weighted gradient-echo MR imaging. *AJNR Am J Neuroradiol.* 2007;28(10):2023-2029.

127. Pratheesh R, Rajaratnam S, Prabhu K, Mani SE, Chacko G, Chacko AG. The current role of transcranial surgery in the management of pituitary adenomas. *Pituitary.* 2013;16(4):419-434.

128. Bahuleyan B, Raghuram L, Rajshekhar V, Chacko AG. To assess the ability of MRI to predict consistency of pituitary macroadenomas. *Br. J. Neurosurg.* 2006;20(5):324-326.

129. Iuchi T, Saeki N, Tanaka M, Sunami K, Yamaura A. MRI prediction of fibrous pituitary adenomas. *Acta Neurochir. (Wien.).* 1998;140(8):779-786.

130. Kanou Y, Arita K, Kurisu K, Tomohide A, Iida K. Clinical implications of dynamic MRI for pituitary adenomas: clinical and histologic analysis. *J. Clin. Neurosci.* 2002;9(6):659-663.

131. Pierallini A, Caramia F, Falcone C, et al. Pituitary macroadenomas: preoperative evaluation of consistency with diffusion-weighted MR imaging--initial experience. *Radiology.* 2006;239(1):223-231.

132. Boxerman JL, Rogg JM, Donahue JE, Machan JT, Goldman MA, Doberstein CE. Preoperative MRI evaluation of pituitary macroadenoma: imaging features predictive of successful transsphenoidal surgery. *AJR Am. J. Roentgenol.* 2010;195(3):720-728.

133. Sumida M, Uozumi T, Mukada K, et al. MRI of pituitary adenomas: the position of the normal pituitary gland. *Neuroradiology.* 1994;36(4):295-297.

134. Sumida M, Uozumi T, Yamanaka M, et al. Displacement of the normal pituitary gland by sellar and juxtasellar tumours: surgical-MRI correlation and use in differential diagnosis. *Neuroradiology.* 1994;36(5):372-375.

135. Fujisawa I, Uokawa K, Horii N, et al. Bright pituitary stalk on MR T1-weighted image: damming up phenomenon of the neurosecretory granules. *Endocr. J.* 2002;49(2):165-173.

136. Smith MV, Laws ER. Magnetic resonance imaging measurements of pituitary stalk compression and deviation in patients with nonprolactin-secreting intrasellar and parasellar tumors: lack of correlation with serum prolactin levels. *Neurosurgery.* 1994;34(5):834-839; discussion 839.

137. Bonneville F, Narboux Y, Cattin F, Rodière E, Jacquet G, Bonneville JF. Preoperative location of the pituitary bright spot in patients with pituitary macroadenomas. *AJNR Am. J. Neuroradiol.* 2002;23(4):528-532.

138. Takahashi T, Miki Y, Takahashi JA, et al. Ectopic posterior pituitary high signal in preoperative and postoperative macroadenomas: dynamic MR imaging. *Eur. J. Radiol.* 2005;55(1):84-91.

139. Saeki N, Hayasaka M, Murai H, et al. Posterior pituitary bright spot in large adenomas: MR assessment of its disappearance or relocation along the stalk. *Radiology*. 2003;226(2):359-365.

140. Eda M, Saeki N, Fujimoto N, Sunami K. Demonstration of the optic pathway in large pituitary adenoma on heavily T2 weighted MR images. *Br. J. Neurosurg.* 2002;16(1):21-29.

141. Sumida M, Arita K, Migita K, Iida K, Kurisu K, Uozumi T. Demonstration of the optic pathway in sellar/juxtasellar tumours with visual disturbance on MR imaging. *Acta Neurochir. (Wien.).* 1998;140(6):541-548.

142. Carrim ZI, Reeks GA, Chohan AW, Dunn LT, Hadley DM. Predicting impairment of central vision from dimensions of the optic chiasm in patients with pituitary adenoma. *Acta Neurochir. (Wien.).* 2007;149(3):255-260; discussion 260.

143. Tokumaru AM, Sakata I, Terada H, Kosuda S, Nawashiro H, Yoshii M. Optic nerve hyperintensity on T2-weighted images among patients with pituitary macroadenoma: correlation with visual impairment. *AJNR Am. J. Neuroradiol.* 2006;27(2):250-254.

144. Saeki N, Uchino Y, Murai H, et al. MR imaging study of edema-like change along the optic tract in patients with pituitary region tumors. *AJNR Am. J. Neuroradiol.* 2003;24(3):336-342.

FIGURES

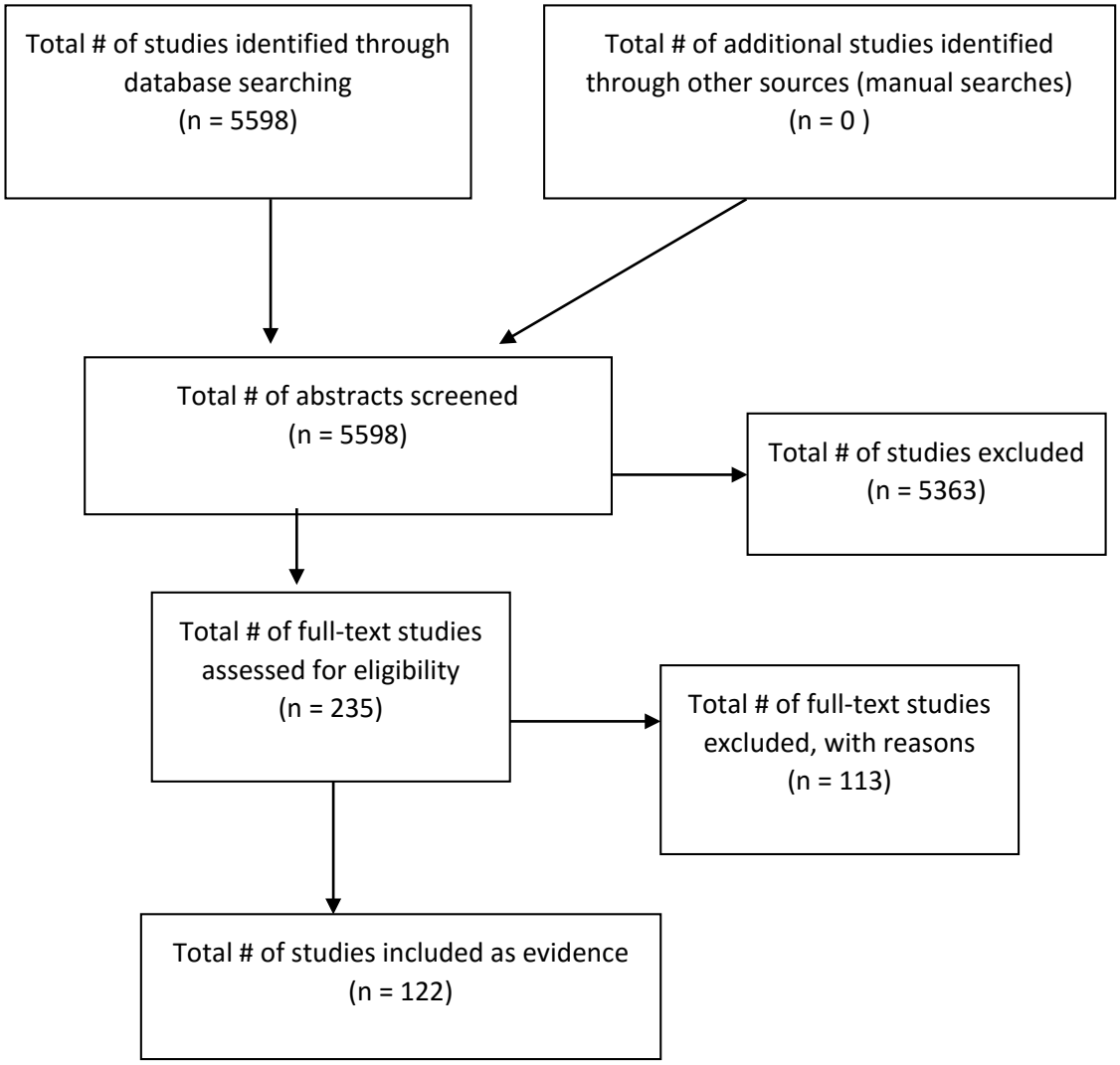

Figure 1: Flow Diagram of Search Results

TABLES

Imaging Modalities Evidence Tables

Table 1 Computed Tomography (CT) Imaging

Author (Year)	Title	Study Description	Number of Patients	Classification Process/Evidence Class	Conclusions
Clark (1986)[9]	Reformatted sagittal images in the differential diagnosis of meningiomas and pituitary adenomas with suprasellar extension.	Clinical experience using coronal reformatted image to discriminate between NFPA and meningiomas.	>100	Diagnostic/ III	Reformatted sagittal images can be used in the differential diagnosis between pituitary tumors with suprasellar extension and meningiomas located in this area.
Chen (1982)[10]	Computed tomography in the diagnosis of pituitary adenoma.	Clinical experience using CT in the diagnosis of pituitary lesions.	85	Diagnostic/ III	There was an abnormal suprasellar cistern in 79. Specifically, the suprasellar cistern was obliterated in 10 cases and had a filling defect in 60 cases. Contrast increases the density of the lesion in 97.6%. The majority of shape of the tumor is round or oval-shaped, sometimes lobulated.

Author (Year)	Title	Study Description	Number of Patients	Classification Process/Evidence Class	Conclusions
Daniels (1981)[11]	Differential diagnosis of intrasellar tumors by computed tomography.	Patients with pituitary adenomas and other sellar/parasellar lesions underwent CT imaging. CT imaging findings including calcifications and low density regions were compared between the different groups of pathologies.	25	Diagnostic/ III	Calcification was a feature of intrasellar meningiomas, aneurysms, and craniopharyngiomas, but not a typical feature of adenomas. Low-density regions representing necrosis or cyst were found in most types of intrasellar tumors. Eccentricity, hyperostosis, and bone destruction were useful signs of aneurysm, meningioma, and metastasis, respectively. Since adenoma cannot always be distinguished from another intrasellar mass, angiography to demonstrate tumor angioarchitecture may be needed to characterize some neoplasms or to confirm an intrasellar aneurysm.
Robertson (1981)[12]	Trends in the radiological study of pituitary adenoma.	Clinical experience using CT for studying pituitary adenomas.	>20	Diagnostic/ III	CT has limited utility in the definitive diagnosis of pituitary lesions.
Gardeur (1981)[13]	CT analysis of intrasellar pituitary adenomas with emphasis on patterns of contrast enhancement.	Patients with pituitary adenomas underwent CT imaging. CT imaging characteristics found in this cohort are described.	85	Diagnostic/ III	Twenty-eight of 85 adenomas exhibited homogeneously increased density. Twenty exhibited heterogeneously increased, patchy, or ringlike density; 16, hypodensity; and 8, isodensity with normal pituitary tissue. In 13 patients, the predominant CT finding was an empty sella with variable enhancement of the adenoma and residual pituitary tissue. CT can visualize adenomas, although there are variations in their appearance.

Author (Year)	Title	Study Description	Number of Patients	Classification Process/Evidence Class	Conclusions
Macpherson (1981)[14]	Radiological differentiation of intrasellar aneurysms from pituitary tumors.	Patients with pituitary adenomas or intrasellar aneurysms underwent CT imaging. Imaging characteristics were compared between the 2 groups of pathologies to identify characteristics diagnostic of each pathology.	35	Diagnostic/ III	A completely eroded area of bone, a completely eroded fossa, a soft tissue opacity in the sphenoid sinus, bilateral displacement of the cavernous sinuses and, on CT, general enlargement of the fossa were seen only with cases of pituitary tumor. CT provides radiologic signs specific to pituitary adenomas.
Hatam (1979)[15]	Diagnosis of sellar and parasellar lesions by computed tomography.	Clinical experience using CT for definitive diagnosis of pituitary lesions.	13	Diagnostic/ III	Pituitary adenomas had higher or equal attenuation relative to brain and had contrast enhancement. These differences can aid in CT based visualization/identification of pituitary adenomas.
Gyldensted (1977)[16]	Computed tomography of intra- and juxtasellar lesions. A radiological study of 108 cases.	Clinical experience using CT and angiography for definitive diagnosis of pituitary lesions.	37	Diagnostic/ III	CT is superior to angiography for the diagnosis of pituitary adenomas.

Author (Year)	Title	Study Description	Number of Patients	Classification Process/Evidence Class	Conclusions
Numaguchi (1981)[17]	Neuroradiological manifestations of suprasellar pituitary adenomas, meningiomas, and craniopharyngiomas.	Patients with pituitary adenomas and other sellar/parasellar lesions underwent CT imaging, skull radiography, and metrizamide cisternography. The various imaging modalities were evaluated for use in diagnosis of each of these pathologies.	16	Diagnostic/ III	The differentiation of different sellar tumors is possible with skull radiography, CT, and cisternography are used. Metrizamide cisternography may be used when the tumor contours are obscure using PIA, or when the differential diagnosis is uncertain after CT.
Hall (1980)[18]	Metrizamide cisternography in pituitary and juxtapituitary lesions.	Patients with pituitary adenomas underwent metrizamide cisternograms. The imaging characteristics are described.	50	Diagnostic/ III	The technique accurately delineates a suprasellar extension of a small or moderate-sized pituitary lesion and usually shows its relationship to the optic chiasm. Large suprasellar masses, however, are not well visualized. Metrizamide cisternography can provide supplemental information relevant to diagnosis of pituitary tumors and is simpler to perform and often better tolerated by patients than is pneumoencephalography.

Author (Year)	Title	Study Description	Number of Patients	Classification Process/Evidence Class	Conclusions
Davis (1985)[19]	CT-surgical correlation in pituitary adenomas: evaluation in 113 patients.	Patients with nonfunctioning pituitary adenomas and secretory adenomas underwent CT imaging. Imaging characteristics were compared between the groups of different pathologies.	17	Diagnostic / III	The 51 functioning and nonfunctioning macroadenomas had similar CT appearances. Only 34 secretory adenomas presented as discrete, focal, hypodense lesions; the rest were isodense with the adjacent pituitary gland. Secretory adenomas were clinically apparent earlier, and, accordingly, the abnormalities seen on CT were less developed. The location of the normal pituitary gland could not be determined by attenuation characteristics; only by infundibulum displacement or opposite to a discrete, focal, hypodense lesion could the gland location be predicted reliably. Adenomas with hemorrhage, infarction, and cyst formation were indistinguishable from those without these findings. CT was helpful in identifying the mass effect of macroadenomas. CT has value in preoperative evaluation of pituitary adenomas, although differentiation of secretory or nonsecretory is not reliable.

Author (Year)	Title	Study Description	Number of Patients	Classification Process/Evidence Class	Conclusions
Sakoda (1981)[20]	CT scan of pituitary adenomas.	Patients with nonfunctioning pituitary adenomas and secretory adenomas underwent CT imaging. CT imaging characteristics including enhancement patterns and cystic component identification were compared between the different groups of pathologies.	17	Diagnostic/ III	The absorption coefficient on contrasting enhanced CT does not identify the specific type of adenoma. Ring-like enhancement was observed in 5 nonfunctioning and 4 PRL-secreting adenomas with suprasellar extension, while cystic components were observed in 4 nonfunctioning and 4 PRL-secreting adenomas. CT scans can visualize both secretory and NFPAs but cannot reliably distinguish between them by radiologic parameters.
Hamid (2008)[22]	Anatomic variations of the sphenoid sinus and their impact on trans-sphenoid pituitary surgery.	Patients with pituitary adenomas had both CT and MR imaging retrospectively evaluated. Different anatomical variations of the sphenoid sinus are described.	296	Prognostic/ III	A highly pneumatized sphenoid sinus may distort the anatomic configuration. CT scans can reliably identify this. The combination of CT and MRI in patients with pituitary adenomas can reliably identify anatomical variations of the sphenoid sinus, which has significant effects on surgical approach.

Author (Year)	Title	Study Description	Number of Patients	Classification Process/Evidence Class	Conclusions
Miki (2007)[23]	Evaluation of pituitary macroadenomas with multidetector-row CT (MDCT): comparison with MR imaging.	Patients underwent multidetector-row CT and conventional MR imaging. Both modalities were evaluated in regard to clarity of tumor margins, identification of normal pituitary gland, identification of erosion or destruction of the sellar floor, and visualization of the adjacent optic pathways.	33	Prognostic/ III	MDCT more clearly demonstrated the lateral tumor margin than MR imaging (*P* = .002). No significant differences in visualization of the normal pituitary gland were noted between MDCT and dynamic MR imaging (*P* = .7). MDCT more clearly demonstrated sellar floor erosion or destruction at the sphenoid sinus than MR imaging (*P* < .001). MR imaging was superior to MDCT for visualizing the adjacent optic pathways (*P* < .001). MDCT is superior to MR imaging for assessing lateral tumor margin and the sellar floor at the sphenoid sinus. MDCT offers useful preoperative information in addition to that obtained from MR imaging.
Abe (2002)[24]	Evaluation of pituitary adenomas by multidirectional multislice dynamic ct.	Clinical experience using multidirectional, multi-splice dynamic CT for visualization of NFPA.	13	Prognostic/ III	The MSDCT-MPR provided the information needed for surgery with good image quality in patients with pacemakers.

Author (Year)	Title	Study Description	Number of Patients	Classification Process/Evidence Class	Conclusions
Lundin (1991)[25]	Comparison of MR imaging and CT in pituitary macroadenomas.	Clinical experience comparing the utility of MR and CT in the study of pituitary lesions.	65	Prognostic/ III	MR was superior to CT except in the demonstration of bone changes and tumor calcification. The superiority of MR was most pronounced regarding cavernous sinus invasion, tumor relationship to the carotid arteries and optic chiasm, and tumor hemorrhage. Extensive bone changes were visualized with both methods; erosions were often seen only with CT. It is concluded that MR is the preferable method for evaluation of pituitary macroadenomas. CT is useful as a supplementary modality when detailed information on bone anatomy is required, particularly if a transsphenoidal surgical approach is contemplated.
Wu W, (1995)[26]	Pituitary microadenoma. MR appearance and correlation with CT.	Clinical experience comparing the utility of MR and CT in the study of pituitary lesions.	20	Prognostic/ III	MR is more sensitive in detection of pituitary lesions, whereas CT is more sensitive to detect sellar floor erosions.

Author (Year)	Title	Study Description	Number of Patients	Classification Process/Evidence Class	Conclusions
Johnson MR, (1992)[27]	The evaluation of patients with a suspected pituitary microadenoma: Computer tomography compared to magnetic resonance imaging.	Clinical experience comparing the utility of MR and CT in the study of pituitary lesions	25	Diagnostic / III	MRI is superior to CT in the assessment of pituitary lesions.

Author (Year)	Title	Study Description	Number of Patients	Classification Process/Evidence Class	Conclusions
Kaufman (1987)[28]	Large pituitary gland adenomas evaluated with magnetic resonance imaging.	Clinical experience using MR for the assessment of NFPAs.	15	Prognostic/ III	Bone destruction and tumor calcification were better detected by CT scanning than by MRI. MRI was as effective as CT scanning in detecting a cyst or variation in tumor consistency. Neither MRI nor CT scanning was capable of distinguishing specific tumor types. In every case, MRI was superior to CT scanning for delineating spatial relationships of the tumor to the 3rd ventricle, the optic apparatus, adjacent brain, and parasellar vasculature. Vessel encasement by tumor was clearly seen on MRI when there was no direct indication of this on other studies. Cavernous sinus invasion was not demonstrated by CT scanning but was indicated by MRI in 5 cases and was surgically confirmed in 3. MRI can provide more precise spatial information on extrasellar tumor extension. When MRI is available, it is the test of choice for the preoperative evaluation of patients with suspected large pituitary gland (sellar region) tumors. Contrast-enhanced CT scanning and angiography can be used as supplementary studies to add information inherently unique to these techniques.

Author (Year)	Title	Study Description	Number of Patients	Classification Process/Evidence Class	Conclusions
Wu (2014)[30]	Usefulness of dual-energy computed tomography imaging in the differential diagnosis of sellar meningiomas and pituitary adenomas: preliminary report.	CT spectral imaging in both the arterial and venous phase were examined for macroadenomas and meningiomas. Normalized iodine concentrations, HU curve slope, and mean CT values of lesions in both the arterial and venous phases were calculated for each group independently. These values were compared between 2 groups using independent sample *t* tests.	33	Diagnostic/ III	Mean CT values using dual-energy CT had 90.9% sensitivity and 100% specificity in differentiating pituitary adenomas from meningiomas. Quantitative dual-energy CT imaging has promising potential for diagnostic differentiation of sellar meningiomas and pituitary adenomas.

Table 2: Magnetic Resonance (MR) Imaging

Author (Year)	Title	Study Description	Number of Patients	Classification Process/Evidence Class	Conclusions
Guy (1991)[31]	A comparison of CT and MRI in the assessment of the pituitary and parasellar region.	Patients with or without pituitary adenomas prospectively underwent both CT and MR imaging. The visualization of the pituitary gland, optic chiasm, and tumor was compared between the 2 modalities.	40	Prognostic/ II	Visualization of the optic chiasm and assessment of displacement of the optic chiasm and the carotid arteries were also better with MRI. CT was equally good at showing cavernous sinus displacement or invasion, sphenoid sinus invasion, and erosion of the floor of the sella turcica, and was the only technique able to show calcification of the gland. The percentage agreement between the observers for the identification of pituitary and parasellar structures was better for MRI than for CT and the clinician in particular found interpretation of the MR images easier. MRI thus not only gives more information overall than CT, but it is a more reliable technique between different observers for the assessment of the pituitary and parasellar region.
Davis (1987)[32]	MR imaging of pituitary adenoma: CT, clinical, and surgical correlation.	Clinical experience comparing MR and CT in the assessment of pituitary lesions.	25	Diagnostic / II	CT was more sensitive than MR for detecting focal lesions (7 vs 3) and sellar-floor erosion (12 vs 6). MR was superior to CT in identifying infundibular abnormalities (7 vs 6), focal abnormalities of the diaphragma sellae (10 vs 7), cavernous sinus invasion (4 vs 2), and optic chiasm compression (6 vs 0). MR may be the procedure of choice for optimal identification and localization of macroadenoma.

Author (Year)	Title	Study Description	Number of Patients	Classification Process/Evidence Class	Conclusions
Lundin (1991)[25]	Comparison of MR imaging and CT in pituitary macroadenomas.	Clinical experience comparing MR and CT in the assessment of pituitary macroadenomas.	65	Prognostic/ III	MR was superior to CT except in the demonstration of bone changes and tumor calcification. The superiority of MR was most pronounced regarding cavernous sinus invasion, tumor relationship to the carotid arteries and optic chiasm, and tumor hemorrhage. Extensive bone changes were visualized with both methods; erosions were often seen only with CT. It is concluded that MR is the preferable method for evaluation of pituitary macroadenomas. CT is useful as a supplementary modality when detailed information on bone anatomy is required, particularly if a transsphenoidal surgical approach is contemplated.

Author (Year)	Title	Study Description	Number of Patients	Classification Process/Evidence Class	Conclusions
Kaufman (1987)[28]	Large pituitary gland adenomas evaluated with magnetic resonance imaging.	Clinical experience using MR for assessing pituitary macroadenomas.	15	Prognostic/ III	Bone destruction and tumor calcification were better detected by CT scanning than by MRI. MRI was as effective as CT scanning in detecting a cyst or variation in tumor consistency. Neither MRI nor CT scanning was capable of distinguishing specific tumor types. In every case, MRI was superior to CT scanning for delineating spatial relationships of the tumor to the 3rd ventricle, the optic apparatus, adjacent brain, and parasellar vasculature. Vessel encasement by tumor was clearly seen on MRI when there was no direct indication of this on other studies. Cavernous sinus invasion was not demonstrated by CT scanning, but was indicated by MRI in 5 cases and was surgically confirmed in 3. MRI can provide more precise spatial information on extrasellar tumor extension. When MRI is available, it is the test of choice for the preoperative evaluation of patients with suspected large pituitary gland (sellar region) tumors. Contrast-enhanced CT scanning and angiography can be used as supplementary studies to add information inherently unique to these techniques.

Author (Year)	Title	Study Description	Number of Patients	Classification Process/Evidence Class	Conclusions
Lee (1985)[33]	Sellar and juxtasellar lesion detection with MR.	Clinical experience using MR for assessing pituitary lesions.	21	Prognostic/ III	Although CT scans showed the abnormalities in most cases, MR was superior in delineating distortions of the optic chiasma and other suprasellar structures and in demonstrating the status of the carotid arteries. MR can reveal fat, hematoma, and cyst and can be used to differentiate the pathologic features of many lesions. MR is superior to CT for preoperative evaluation of pituitary adenomas.
Karnaze (1986)[34]	Suprasellar lesions: evaluation with MR imaging.	Clinical experience using MR for assessing pituitary lesions.	15	Prognostic/ III	In comparing MR and CT images, MRI superior in 5, MR equal in 10, CT superior in 0. MR was equivalent to CT in allowing lesions to be detected, and several cases more accurately defined altered perisellar anatomy. Vascular abnormalities can be better evaluated with MR, and use of angiography can be avoided in some cases.
Mikhael (1988)[35]	MR imaging of pituitary tumors before and after surgical and/or medical treatment.	Clinical experience using MR for assessing pituitary lesions.	26	Diagnostic/ III	MR was more accurate than CT at diagnosis of pituitary adenomas. Hemorrhage in pituitary tumors was easily seen on MR and missed on CT.

Author (Year)	Title	Study Description	Number of Patients	Classification Process/Evidence Class	Conclusions
Gutenberg (2009)[37]	A radiologic score to distinguish autoimmune hypophysitis from nonsecreting pituitary adenoma preoperatively.	MR imaging of patients with either nonfunctioning pituitary adenomas or autoimmune hypophysitis were compared based on 16 morphological features in addition to sex, age, and pregnancy status. The significant predictors were analyzed in a multiple logistic regression model to identify a radiologic score to predict nonfunctioning pituitary adenomas before surgery.	98	Diagnostic/ III	The diagnostic score had a global performance of 0.9917 and correctly classified 97% of the patients, with a sensitivity of 92%, a specificity of 99%, a positive predictive value of 97%, and a negative predictive value of 97% for the diagnosis of AH. This new radiologic score could be integrated into the management of patients with AH, who derive greater benefit from medical as opposed to surgical treatment.
Kucharczyk (1986)[38]	Pituitary adenomas: high-resolution MR imaging at 1.5 T.	Clinical experience using 1.5 T MR for assessing pituitary lesions.	17	Diagnostic/ III	All of the macroadenomas were accurately localized and their extent delineated, particularly on T1-weighted coronal sections. Adenomas typically appeared hypointense on T1-weighted coronal sections. The appearance on T2-weighted images was variable, and generally the lesions were less well seen. Involvement of parasellar structures, particularly the optic chiasm and cavernous sinuses, was accurately depicted. Cyst formation and hemorrhage could be characterized in some instances. MR imaging is an excellent modality for preoperative localization and identification of pituitary adenomas.

Author (Year)	Title	Study Description	Number of Patients	Classification Process/Evidence Class	Conclusions
Steiner (1989)[39]	Gd-DTPA enhanced high resolution MR imaging of pituitary adenomas.	Clinical experience using Gd-DTPA for assessing pituitary lesions.	38	Diagnostic/ III	Compared with the normal pituitary anterior lobe, 8% of the adenomas were hyperintense, 45% were isointense, 42% were hypointense, and 5% were inhomogeneously intense. After Gd-DTPA administration, 13% enhanced to a greater degree, 10% to the same, and 57% to a lesser degree than the normal pituitary tissue. Twenty percent showed inhomogeneous enhancement. In 10%, there was evidence of adenoma only in the enhanced images. The delineation of the adenoma from the cavernous sinus was improved from 47% in unenhanced scans to 91% after Gd-DTPA administration. With 1.5 T spin echo MR imaging, contrast administration leads to improvements in diagnosis and visualization of pituitary adenoma and should be a part of pituitary radiologic investigation.

Author (Year)	Title	Study Description	Number of Patients	Classification Process/Evidence Class	Conclusions
Steiner (1994)[40]	MR-appearance of the pituitary gland before and after resection of pituitary macroadenomas.	Clinical experience using MRI for assessing the pre- and postoperative appearances of pituitary lesions.	30	Diagnostic/ III	On preoperative MR images, contrast administration increased the detectability of the anterior lobe from 30% to 80%. Depending on the size and extension of the adenoma, the pituitary gland was displaced to the suprasellar space (53%) and/or deformed to a club-shaped (27%) or sickle-shaped (47%) configuration. In 6 patients, the sickle-shaped pituitary gland was interposed between the cavernous sinus and the adenoma ("rim-sign"), which was seen only on gadopentetate dimeglumine-enhanced images. In these cases, there was no infiltration of the cavernous sinus at surgery. Postoperatively, descent of the pituitary gland was found in 63% and re-expansion in 54%. We conclude that contrast administration improves the detectability of the pituitary gland on preoperative MR images and that the displacement and deformation of the pituitary gland depend on the size, location, and extension of the adenoma. Preoperatively, demonstration of the pituitary gland interposed between the cavernous sinus and the adenoma ("rim-sign") is a very useful sign for exclusion of cavernous sinus infiltration, best seen on contrast-enhanced coronal MR images.

Author (Year)	Title	Study Description	Number of Patients	Classification Process/Evidence Class	Conclusions
Hayashi (1995)[41]	Dynamic MRI with slow injection of contrast material for the diagnosis of pituitary adenoma.	Clinical experience using dynamic MRI for assessing pituitary lesions.	14	Diagnostic / III	The most remarkable contrast between adenoma and normal tissue was obtained from the fourth to eighth images. In other words, we could obtain the strongest contrast at 144.8 to 299.6 seconds from the start of contrast injection. Slow injection suggests that stronger images can be obtained a longer period after contrast injection, defining differences in contrast enhancement between normal tissue and pituitary adenomas.
Hald (1994)[42]	MR imaging of pituitary region lesions with gadodiamide injection.	Clinical experience using gadodiamide MRI for assessing pituitary lesions	12	Diagnostic/ III	No additional diagnostic information was obtained using 0.3 mM/kg gadodiamide injection compared to 0.1 mM/kg gadopentate dimeglumine in the same patients. The high dose (0.3 mM/kg) gadodiamide injection in 7 patients did not shorten the T2 value sufficiently to overwhelm the T1 shortening and leave pathologic lesions hypointense compared to precontrast studies. Consistent with previous reports, gadodiamide injection was found to be a safe and effective contrast medium for MR imaging of the pituitary region, and this was not dependent on levels of contrast. With the comparable relaxivities of gadodiamide injection and gadopentetate dimeglumine, similarities in results have to be expected when using these media for MR image enhancement.

Author (Year)	Title	Study Description	Number of Patients	Classification Process/Evidence Class	Conclusions
Davis (1991)[43]	Pituitary adenoma: correlation of half-dose gadolinium-enhanced MR imaging with surgical findings in 26 patients.	Clinical experience using half-dose gadolinium MRI for assessing pituitary lesions.	12	Diagnostic/ II	The high signal intensity of the posterior pituitary and of intrasellar hemorrhage was obscured on postcontrast studies. Delayed images proved unnecessary. This prospective evaluation suggests that a half-dose study is comparable to retrospective studies, in which full-dose techniques were used for detection of micro- and macroadenomas. Imaging times are reasonably short, and cost of contrast material is potentially reduced.
Cury (2009)[44]	Non-functioning pituitary adenomas: clinical feature, laboratorial and imaging assessment, therapeutic management and outcome.	Patients with nonfunctioning pituitary adenomas were retrospectively analyzed and results of biochemical evaluation, radiologic studies, visual studies, and management are described.	104	Diagnostic/ III	Preoperative imaging classified 93% of the tumors as macroadenomas. MR preoperative imaging can reliably identify NFPAs.

Author (Year)	Title	Study Description	Number of Patients	Classification Process/Evidence Class	Conclusions
Lundin (1992)[45]	Gd-DTPA-enhanced MR imaging of pituitary macroadenomas.	Patients with nonfunctioning pituitary adenomas and secretory adenomas were evaluated with conventional MR imaging with and without contrast enhancement. The pre- and post-contrast images were compared, as well as between the different groups of pathologies.	40	Diagnostic/ III	Compared with pre-contrast T1-weighted images only, post-contrast images provided considerable additional information; but, not infrequently, this information could also be extracted from pre-contrast T2-weighted images. Post-contrast images were superior regarding the tumor relationship to the cavernous sinus and to the normal pituitary tissue. T2-weighted images were helpful in the diagnosis of degenerative changes, in particular intratumoral hemorrhage. A positive correlation was found between the T2 value (from dual echo sequences) and the degree of enhancement in areas with an appearance of solid tumor tissue, and the enhancement was significantly lower in GH-secreting tumors than in non-secreting ones. The use of Gd-DTPA is often justified in pituitary macroadenomas, particularly in preoperative evaluation.

Table 3: 1.5 versus 3T Scanners

Author (Year)	Title	Study Description	Number of Patients	Classification Process/ Evidence Class	Conclusions
Sekiya (1985)47	Magnetic resonance imaging of the normal pituitary gland and pituitary adenoma: preliminary experience with a resistive magnet.	Clinical experience using MRI to assess pituitary lesions.	12	Diagnostic / III	Adenomas that showed extrasellar extension together with surrounding structures were well demonstrated on sagittal and coronal scans. It can be expected that with further technical developments, MR imaging will play an important role in the clinical management of pituitary adenomas.
Oot (1984)48	MR imaging of pituitary adenomas using a prototype resistive magnet: preliminary assessment.	Clinical experience using MRI to assess pituitary lesions.	10	Diagnostic / III	The larger adenomas were identified readily by MR imaging, which, unlike CT, suggested old tumor hemorrhage in 2 cases, which was confirmed at surgery and histologic examination. MR and CT images were also compared for relative effectiveness in identifying important perisellar structures.

Pinker (2005)49	The value of high-field MRI (3T) in the assessment of sellar lesions.	Patients underwent both conventional MR and high-field MR images using a 3T scanner. A RARE sequence was used for T2-weighted images and a 3D gradient echo sequence was used for T1-weighted images. These high field images were compared to conventional MR images.	16	Diagnostic / III	Sensitivity to infiltration was 83% for 3T and 67% for standard MRI. Specificity was 84% for 3T and 58% for standard MRI. The segments of the cranial nerves were seen as mean 4 hypointense spots (range 2-5 spots) on high-field MRI in contrast to 3 spots (range 0-4 spots) on standard MRI. This difference was considerably significant ($P < .001$, Wilcoxon rank sum test). High-field MRI is superior to standard MRI for the prediction of invasion of adjacent structures in patients with pituitary adenomas and improves surgical planning of sellar lesion.
Wolfsberger (2004)50	Application of three-tesla magnetic resonance imaging for diagnosis and surgery of sellar lesions.	Clinical experience using 3T MRI to assess pituitary lesions.	21	Diagnostic / III	3T is superior to standard 1.5T for the delineation of parasellar anatomy and tumor infiltration of the cavernous sinus.

Table 4: Specific MR Sequences

Author (Year)	Title	Study Description	Number of Patients	Classification Process/ Evidence Class	Conclusions
Davis (2013)[51]	Evaluation of the pituitary gland using magnetic resonance imaging: T1-weighted vs VIBE imaging.	Patients underwent both coronal T1-weighted and volumetric interpolated breath-hold examination imaging (VIBE). The 2 sequences were compared in terms of contrast enhancement, cavernous sinus appearance, and optic chiasm appearance. For each subject, VIBE was rated as better, equal, or worse to T1-weighted images and statistically compared using chi-square tests. These comparisons were also made while stratifying for macroadenomas and post-surgical patients.	32	Diagnostic / III	There was a trend to VIBE being superior to T1W for visualization of pituitary adenomas, but these data were not statistically significant. Visualization of chiasm in macroadenomas was similar for both techniques. VIBE was significantly superior to T1W with respect to pituitary and cavernous sinus contrast enhancement and cavernous sinus anatomy. Although not statistically significant, VIBE may improve the resolution of MR images for preoperative visualization of pituitary adenomas, cavernous sinus invasion, and optic chiasm compression. This strength may be even larger with higher tesla magnets.

Yamamoto (2014)[53]	Tumor consistency of pituitary macroadenomas: predictive analysis on the basis of imaging features with contrast-enhanced 3D FIESTA at 3T.	Patients underwent both conventional MRI and contrast-enhanced 3D FIESTA sequences preoperatively. Two neuroradiologists evaluated MR imaging findings, specifically those on the FIESTA scan. During surgery, neurosurgeons classified the tumors as soft or hard. Postoperatively, collagen content and residual tumor size was calculated. Fisher exact probability tests and independent sample *t* tests were used to compare predictions of MR imaging findings to intraoperative tumor consistency, tumor collagen content, and postoperative tumor size.	29	Diagnostic / III	Sensitivity and specificity were higher for contrast-enhanced FIESTA (1.00 and 0.88-0.92, respectively) than for contrast-enhanced T1WI (0.80 and 0.25-0.33, respectively) and T2WI (0.60 and 0.38-0.54, respectively). Compared with mosaic-type adenomas, solid-type adenomas tended to have a hard tumor consistency as well as a significantly higher collagen content and lower postoperative tumor size. Contrast-enhanced FIESTA can provide preoperative characterization of the consistency of pituitary adenomas.
Rofsky (1999)[54]	Abdominal MR imaging with a volumetric interpolated breath-hold examination.	Clinical experience using VIBE MRI for assessment of pituitary lesions	20	Prognostic / III	VIBE offer superior resolution of anatomic structures relative to conventional MRI.

Davis (2013)[51]	Evaluation of the pituitary gland using magnetic resonance imaging: T1-weighted vs VIBE imaging.	Patients underwent both coronal T1-weighted and volumetric interpolated breath-hold examination imaging (VIBE). The 2 sequences were compared in terms of contrast enhancement, cavernous sinus appearance, and optic chiasm appearance. For each subject, VIBE was rated as better, equal, or worse to T1-weighted images and statistically compared using chi-square tests. These comparisons were also made while stratifying for macroadenomas and post-surgical patients.	32	Prognostic / III	There was a trend to VIBE being superior to T1W for visualization of pituitary adenomas, but these data were not statistically significant. Visualization of chiasm in macroadenomas was similar for both techniques. VIBE was significantly superior to T1W with respect to pituitary and cavernous sinus contrast enhancement and cavernous sinus anatomy. Although not statistically significant, VIBE may improve the resolution of MR images for preoperative visualization of pituitary adenomas, cavernous sinus invasion, and optic chiasm compression. This strength may be even larger with higher tesla magnets.

Cao (2013)[55]	Magnetic resonance imaging appearance of the medial wall of the cavernous sinus for the assessment of cavernous sinus invasion by pituitary adenomas.	Patients underwent MRI with both conventional and proton density weighted images preoperatively. The appearance and invasion of medial wall of the cavernous sinus in the proton density weighted scans was compared to the Knosp grading system, percentage encasement of the internal carotid artery, and replacement of cavernous sinus compartment criteria on conventional MR scans, surgical findings, and Ki-67 labeling index results.	48	Prognostic / III	The sensitivity of MRI visualization of the medial wall of the cavernous sinus for detection of CSI was 93.3% with a specificity of 93.8%, which was significantly higher than other preoperative radiologic signs including KGS, PEICA, and RCSC (P = .007, P = 0.008, and P = .056, respectively). Histopathological results showed no significant differences between MRI visualization of the MWCS and the Ki-67 LI. Proton density weighted scans can permit adequate visualization of the medial wall of the cavernous sinus. This sign was found to be the best in comparison to other radiologic signs with conventional MRI. This new type of scan may be the best way of identifying if tumor invades the cavernous sinus.

Mahmoud (2010)[57]	Role of PROPELLER diffusion weighted imaging and apparent diffusion coefficient in the diagnosis of sellar and parasellar lesions.	Patients with conventional MR and periodically rotated overlapping parallel lines with enhanced reconstruction (PROPELLER) diffusion weighted imaging were retrospectively analyzed. ADC values were calculated from the PROPELLER scans. DC values for pituitary adenomas and other sellar mass lesions were analyzed using intraoperative and histological diagnoses as the gold standard.	38	Diagnostic / III	ADC-MIN of hemorrhagic pituitary adenomas was lower than of the other lesions with similar appearance on conventional MRI (non-hemorrhagic pituitary adenomas, craniopharyngiomas, Rathke's cleft cysts; accuracy 100%); the useful cut-off value was 0.700 x 10(-3)mm(2)/s. ADC-MAX of meningiomas was lower than of non-hemorrhagic pituitary adenomas (accuracy 90.3%; *P* < .01). ADC-MIN of craniopharyngiomas was lower than of Rathke's cleft cysts (accuracy 100%; *P* < .05). As PROPELLER DWI can be useful in the examination of sellar and parasellar lesions, calculation of the ADC values helps to differentiate between various sellar and parasellar lesions.

Bladowska (2013)[60]	Usefulness of perfusion weighted magnetic resonance imaging with signal-intensity curves analysis in the differential diagnosis of sellar and parasellar tumors: preliminary report.	Patients underwent both conventional MRI and perfusion weighted MR imaging. Mean and maximum values of relative cerebral blood volume, relative peak height, and relative percentage of signal intensity recovery were calculated from the perfusion weighted MR images. These parameters were compared between different pathologies (pituitary macroadenomas, meningiomas, craniopharyngioma, hemangioblastoma, glioma, and metastasis).	23	Diagnostic / III	There were statistically significant differences in the mean and maximum rCBV values (P = .026 and P = .019, respectively). The maximum rCBV values >7.14 and the mean rCBV values >5.74 with the typical perfusion curve were very suggestive of the diagnosis of meningioma. Perfusion weighted MR imaging can provide supplemental information to differentiate pituitary adenomas from meningiomas. However, it is unclear how this improves the sensitivity and specificity of diagnosis of sellar/parasellar tumors.
Manfre (1997)[61]	Perfusion MRI in normal and abnormal pituitary gland. A preliminary study.	Patients with pituitary adenomas, other sellar/parasellar pathology, and non-tumor controls underwent perfusion MR imaging. Differences in maximal contrast percentual variation, timing of enhancement, and patterns of enhancement were compared between the different groups of pathologies.	13	Diagnostic / III	The timing of enhancement in normal patients matched perfectly with normal pituitary vascularization, while there was abnormal timing in pathological condition. These tumors had significant enhancement either simultaneously or in the frame after the enhancement of the dural sinuses. Pituitary adenomas have specific characteristics on perfusion MRI.

Sakai (2013)[62]	Arterial spin-labeled perfusion imaging reflects vascular density in nonfunctioning pituitary macroadenomas.	Patients underwent both conventional MR imaging and arterial spin-labeled perfusion imaging. Degree of enhancement was calculated by dividing the signal intensity on T1-weighted with contrast to the T1-weighted without contrast. Normalized tumor blood flow values were calculated by dividing the mean value of the tumor region of interest by mean region of interest values in the cerebellar hemispheres. Relative microvessel attenuation was calculated by dividing the total microvessel wall area by entire CD31 stained tissue area. These parameters were compared with each other as well as the presence of intra- or postoperative hemorrhage by surgeon visualization.	11	Prognostic / III	A statistically significant difference in normalized tumor blood flow values was observed visually between the intraoperative hypovascular and hypervascular groups ($P < .05$). One of these hypervascular cases actually did have symptomatic postoperative hemorrhage. ASL perfusion imaging can reflect the vascular density of NFPAs and may be a viable test in predicting intra/postoperative tumor hemorrhage.

Mahmoud (2011)[63]	Role of PROPELLER diffusion-weighted imaging and apparent diffusion coefficient in the evaluation of pituitary adenomas.	Patients who underwent conventional MR and periodically rotated overlapping parallel lines with enhanced reconstruction (PROPELLER) DWI were retrospectively analyzed. Mean, max, and min values from the PROPELLER DWI images were calculated. Intraoperative tumor consistency was recorded by neurosurgeons. ADC values were compared to tumor consistency experienced intraoperatively and percent collagen content.	19	Prognostic / III	Tumor consistency was strongly associated with the percent collagen content. However, neither the tumor consistency nor the percent collagen content was correlated with MRI findings or ADC values. The SI of growth hormone-producing adenomas on T2-WI was lower than that of the other pituitary adenomas studied ($P < .01$); no other significant difference was found in the ADC or on conventional MRI between pituitary adenomas with different secretory functions. The MIB-1 LI of pituitary adenomas was not correlated with their appearance on conventional MRI or their ADC values. Unlike other studies, this study found tumor consistency was not correlated with ADC findings.
Suzuki (2007)[64]	Apparent diffusion coefficient of pituitary macroadenoma evaluated with line-scan diffusion-weighted imaging.	Patients prospectively underwent line-scan diffusion weighted imaging (LSDWI) and had ADC values calculated. These ADC values were correlated with the consistency recorded at surgery.	19	Prognostic / II	A soft consistency was found at surgery in 13 patients (mean ADC: 0.84+/-0.1x10(-3) mm2/s); an intermediate consistency was observed in 6 patients (mean ADC: 0.81+/-0.16x10(-3) mm2/s). No tumors of hard consistency were found. There was no significant difference in ADC values between tumors of soft consistency compared with tumors of intermediate consistency ($P = 0.37$). A relationship between tumor consistency and the ADCs of soft and intermediate macroadenomas was not shown in this study using LSDWI.

Table 5: Positron Emission Tomography (PET) Imaging

Author (Year)	Title	Study Description	Number of Patients	Evidence Class	Conclusions
Jeong (2010)[67]	Incidental pituitary uptake on whole-body 18f-fdg pet/ct: a multicentre study.	Determine the incidence of incidental pituitary uptake on whole-body 18F-fluorodeoxyglucose (FDG) positron emission tomography/computed tomography (PET/CT).	40967	Diagnostic / III	Focally increased pituitary FDG uptake on PET/CT was found in 30 of 40967 patients, accounting for an incidence of 0.073%.
Hyun (2011)[68]	Incidental focal 18F-FDG uptake in the pituitary gland: clinical significance and differential diagnostic criteria.	Patients with (18)F-FDG PET/CT were retrospectively evaluated for pituitary gland uptake. Receiver-operating-characteristic curve analysis was used to determine a cutoff for pathologic or physiologic uptake.	21	Diagnostic / III	Incidental pituitary uptake was macroadenomas (n = 21) after incidental pituitary uptake in 13145 consecutive patients. When a maximum standardized uptake value of 4.1 was used as an optimal criterion for detecting pathologic uptake, the diagnostic sensitivity, specificity, and accuracy were 96.6%, 88.1%, and 91.5%, respectively to identify pituitary adenomas. Although not commonly carried out, FDG PET may be able to identify pituitary adenomas using certain max standardized uptake values.

Author (Year)	Title	Study Description	Number of Patients	Evidence Class	Conclusions
Seok (2013)[69]	Analysis of 18F-fluorodeoxyglucose positron emission tomography findings in patients with pituitary lesions.	Patients underwent both conventional MR and (18)F-fluorodeoxyglucose positron emission tomography imaging (FDG PET). Conventional imaging findings were compared to FDG uptake patterns, using maximum standardized uptake values. FDG uptake patterns were compared in patients with micro- and macroadenomas.	24	Diagnostic / III	All patients with pituitary macroadenomas showed increased (18)F-FDG uptake on PET scans. Meanwhile, only 5 (50%) of the 10 patients with pituitary microadenomas showed positive PET scans. For positive (18)F-FDG uptake, maximum standardized uptake values (SUV(max)) > 2.4 had 94.7% sensitivity and 100% specificity. PET can be used as a supplementary tool for identifications of pituitary adenomas as a whole.

Author (Year)	Title	Study Description	Number of Patients	Evidence Class	Conclusions
Lucignani (1997)[70]	Differentiation of clinically non-functioning pituitary adenomas from meningiomas and craniopharyngiomas by positron emission tomography with [18F]fluoro-ethyl-spiperone.	Patients with nonfunctioning pituitary adenomas, craniopharyngiomas, or meningiomas underwent [18F]fluoro-ethyl-spiperone (FESP) positron emission tomography (PET). Differences in visual interpretation of the PET images were compared between the different groups of pathologies.	16	Diagnostic / III	The results demonstrated that PET with [18F]FESP is a very specific method for differentiating adenomas from craniopharyngiomas and meningiomas. The visual interpretation of images allows such differentiation at approximately 70 minutes after tracer injection. Semiquantitative analysis of the dynamic PET data confirmed the results of visual interpretation, demonstrating that the uptake of [18F]FESP was consistently (ie, throughout the series) at least two- to three-fold higher in non-functioning adenomas than in other parasellar tumors as early as 70 minutes after tracer injection, and that it increased still further thereafter. It is concluded that PET with [18F]FESP might be of clinical value in those cases in which the differential diagnosis among various histological types of sellar tumor is uncertain with conventional methods.

Author (Year)	Title	Study Description	Number of Patients	Evidence Class	Conclusions
Bergstrom (1991)[71]	PET as a tool in the clinical evaluation of pituitary adenomas.	Patients with pituitary adenomas and other sellar lesions underwent positron emission tomography (PET) with carbon 11-methionine and/or dopamine D2 receptor ligands. Uptake ratios were compared between the different types of tumors.	400	Diagnostic / III	PET with carbon-11-methionine can give valuable complementary information in the diagnosis of this tumor due to PET's ability to adequately depict viable tumor tissue in contrast to fibrosis, cysts, and necrosis. Furthermore, PET with dopamine D2 receptor ligands can characterize the degree of receptor binding and thus give information as to the prerequisites for dopamine agonist treatment. Most important is the very high sensitivity given by PET with carbon-11-methionine in the evaluation of treatment effects. PET can be used as a supplement to MR for the diagnosis for pituitary adenoma as well as a sense of histology in terms of dopamine receptors.

Table 6: Single-Photo Emission Computed Tomography (SPECT) Imaging

Author (Year)	Title	Study Description	Number of Patients	Evidence Class	Conclusions
de Herder (1999)[72]	Comparison of iodine-123 epidepride and iodine-123 IBZM for dopamine D2 receptor imaging in clinically non-functioning pituitary macroadenomas and macroprolactinomas.	Patients with nonfunctioning pituitary adenomas and prolactinomas underwent pituitary iodine-123-epidepride single photon emission tomography (SPET) and 123I-IBZM SPET. The uptake of radioactivity was determined using a visual scoring system. The uptake index was calculated by dividing the average count rates in the pituitary region by the average count rates in the cerebellum. The uptake levels and uptake index was compared between the 2 groups of pathologies.	15	Diagnostic / III	Specific binding of 123I-epidepride was demonstrated in 9 of the 15 clinically non-functioning pituitary adenomas (60%), but specific binding of 123I-IBZM was shown in only 6 of these 15 cases (40%). The uptake of 123I-epidepride in the pituitary region was consistently higher than that of 123I-IBZM. None of the patients who showed absence of uptake of 123I-epidepride in the pituitary area showed uptake of 123I-IBZM in this area. 123I-epidepride SPET is superior to 123I-IBZM SPET for the visualization of dopamine receptor-positive pituitary adenomas. 123I-epidepride SPET potentially might serve to predict the response of clinically non-functioning pituitary adenomas to dopamine agonist therapy.

Author (Year)	Title	Study Description	Number of Patients	Evidence Class	Conclusions
Kojima (2001)[73]	Is technetium-99m-MIBI taken up by the normal pituitary gland? A comparison of normal pituitary glands and pituitary adenomas.	Patients with and without pituitary adenomas underwent both conventional MR and technetium-99m-hexakis-2-methyoxy-isobutyl-isonitril single photon emission computed tomography (SPECT) imaging. SPECT uptake shape and location patterns were compared between patients with tumors and normal controls.	15	Diagnostic / III	Analysis of the uptake showed that 10 (67%) adenomas were C, and 5 (33%) were LO. Of the controls, 5 (33%) were C, and 10 (69%) were T/R. With regard to location, all patients with pituitary adenomas were classified as P, and all control subjects (93%) but one showed uptake in the dorsum sellae and clivus (D/C). MIBI was taken up in the dorsum sellae or clivus but not the normal pituitary gland and had a strong affinity for the pituitary adenoma. MIBI SPECT may be a useful auxiliary examination technique for the location diagnosis of pituitary adenoma.
Yamamura (2003)[74]	Differentiation of pituitary adenomas from other sellar and parasellar tumors by 99mTc(V)-DMSA scintigraphy.	Patients with pituitary adenomas and other sellar/parasellar lesions underwent pentavalent technetium-99m dimercaptosuccinic acid scintigraphy. Imaging findings were compared by differing pathology.	21	Diagnostic / III	99mTc(V)-DMSA scintigraphy showed overall sensitivity of 81% (17/21 cases) for detecting pituitary adenomas, in particular 100% for non-functioning adenomas. 99mTc(V)-DMSA may be useful for detecting pituitary adenomas, especially non-functioning adenomas, and for the differentiation of non-functioning pituitary adenomas from other sellar and parasellar lesions.

Author (Year)	Title	Study Description	Number of Patients	Evidence Class	Conclusions
Lastoria (1995)[75]	Technetium-99m pentavalent dimercaptosuccinic acid imaging in patients with pituitary adenomas.	Patients with nonfunctioning pituitary adenomas, secretory adenomas, or non-tumor controls underwent technetium-99m-labeled pentavalent dimercaptosuccinic acid scintigraphy. Uptake levels were compared between the different groups of pathologies.	15	Diagnostic / III	Seventeen GH-secreting (81%), 7 PRL-secreting (78%), 3 ACTH-secreting (50%), 15 non-functioning (100%), and 1 (50%) mixed adenoma significantly concentrated [99mTc](V)DMSA, showing elevated tumor-to-background (T/B) ratios. Non-adenomatous lesions of the sella turcica did not concentrate [99mTc](V)DMSA in the pituitary as well as brain tumors and 8 out of 10 metastatic thyroid cancers. The [99mTc](V)DMSA scintigraphy showed an overall sensitivity of 81% (43/53) in detecting pituitary adenomas, which was increased to 95% for lesions greater than 10 mm in size. High-quality images with minimal total body radiation were obtained, enabling a good in vivo characterization of viable adenomatous tissue as well as an accurate monitoring of the effects of different therapeutic regimens. Technetium-99m DMSA may be used as a supplementary tool in the preoperative identification of pituitary adenoma.

Author (Year)	Title	Study Description	Number of Patients	Evidence Class	Conclusions
Colao (1999)[76]	The pituitary uptake of (111)In-DTPA-D-Phe1-octreotide in the normal pituitary and in pituitary adenomas.	Clinical experience using The (111)In-DTPA-D-Phe1-octreotide for assessment of pituitary lesions.	38	Diagnostic / III	The (111)In-DTPA-D-Phe1-octreotide uptake in pituitary adenomas was significantly correlated to octreotide treatment. Pituitary (111)In-DTPA-D-Phe1-octreotide uptake was clearly detectable in 40% of patients with SS-ET not located in the pituitary region at 24 hours post-injection. (111)In-DTPA-D-Phe1-octreotide scintigraphy with late pituitary images cannot be considered a useful method to predict the chronic responsiveness to octreotide in individual patients.

Author (Year)	Title	Study Description	Number of Patients	Evidence Class	Conclusions
Oppizzi (1998)[77]	Scintigraphic imaging of pituitary adenomas: an in vivo evaluation of somatostatin receptors.	Patients with nonfunctioning pituitary adenomas, GH-secreting adenomas, or no tumor underwent pituitary scintigraphy with somatostatin analog pentetreotidean. The accumulation of this analog was expressed as an activity radio between the uptake of radioactivity by the adenoma to that of normal brain tissue. Activity ratios were compared between the different groups of pathologies.	22	Diagnostic / III	In 15 out of the 17 patients with GH-secreting adenoma, an accumulation of the radioligand was shown. Median activity ratio was 3.8 (range 1-6.9; in 14 AR were greater than 2.2) and ARs were directly correlated ($r = 0.54$; $P < .05$) with the suppressibility of plasma GH levels by octreotide (OC) acute administration. In 2 patients who repeated scintigraphy during chronic OC treatment, AR values were reduced. In all the 22 patients with NFPA, an accumulation of 111In-P at the pituitary level was observed and median AR was 3.0 (range 1.5-20; in 14 greater than 2.2). In vitro autoradiography of surgical specimens in 6 NFPA patients revealed SS-R in 4 cases with high scintigraphic AR and negative results in 2 cases with low AR. Scintiscan was repeated during chronic OC treatment in 5 patients with high score: AR decreased in 1 patient, increased in 3, and did not change in the other patient. No changes in tumor size were shown in any of these patients. A total of 8 patients (3 GH secreting and 5 NFPA) had "normal" AR values. In acromegaly scintigraphy with 111In-P visualizes functioning pituitary SS-R coupled to intracellular events that control hormonal hypersecretion and tumor growth. In contrast, in spite of the positivity of 111In-P imaging in most patients with NFPA, their receptors might have a defect in the coupling-transduction process, as they are not inhibited by OC treatment and no tumor shrinkage is observed.

Author (Year)	Title	Study Description	Number of Patients	Evidence Class	Conclusions
Broson-Chazot (1997)[78]	Somatostatin receptor imaging in somatotroph and non-functioning pituitary adenomas: correlation with hormonal and visual responses to octreotide.	Patients with nonfunctioning pituitary adenomas and GH-secreting adenomas underwent somatostatin receptor scintigraphy. Uptake index was calculated and a threshold for a positive test was calculated using non-tumor controls. Uptake index data was compared in the different groups of pathologies.	29	Prognostic / III	In non-functioning pituitary adenomas, somatostatin receptor scintigraphy was positive in 62%. Based on visual effects, the positive predictive value was 61% and the negative predictive value was 100%. A wide distribution of somatostatin binding sites was found in 8 non-functioning pituitary adenomas with expression of sst2 only. In patients with non-functioning pituitary adenomas, negative somatostatin receptor scintigraphy predicts that there will be no visual improvement during octreotide treatment.
Rieger (1997)[79]	Somatostatin receptor scintigraphy in patients with pituitary adenoma.	Clinical experience using somatostatin receptor scintigraphy for the assessment of pituitary lesions.	42	Diagnostic / III	No specific binding of 111In-octreotide was found. Five patients showed a weak positive, 5 had a positive, and 9 a strong positive signal in the region of interest. Uptake of octreotide was significantly correlated with tumor size and age ($P < .01$).

Author (Year)	Title	Study Description	Number of Patients	Evidence Class	Conclusions
de Herder (1996)[80]	In vivo imaging of pituitary tumours using a radiolabelled dopamine D2 receptor radioligand.	Patients with nonfunctioning pituitary adenomas and secretory adenomas underwent pituitary dopamine D2 receptor scintigraphy with (S)-2-hydroxy-3-123I-iodo-6-methoxy-N-[(1-ethyl-2-pyrrolidinyl) methylbenzamide and single photon emission tomography. Imaging findings were compared for the different groups of pathologies.	17	Diagnostic / III	Single-photon emission tomography (SPECT) showed significant uptake of 123I-IBZM in the pituitary region in 3/5 macroprolactinoma patients. In 4/17 patients with NFPA, significant uptake of the radioligand in the pituitary region was observed. In 2/3 scan-positive NFPA patients who were treated with quinagolide, shrinkage of the pituitary tumors was observed. Treatment with quinagolide resulted in stabilization of tumor growth in the other scan-positive patients. Four out of 17 patients with NFPA and a negative SPECT were treated with quinagolide. Tumor growth was observed in 1 patient, and tumor size did not change in the other 3 patients. The pituitary region of none of the 12 acromegaly patients showed significant uptake of 123I-IBZM. Sensitivity of the GH-secreting adenomas to quinagolide was demonstrated in 8/12 patients in vivo by an acute test, and in 6/9 of the tumors in vitro. Pituitary SPECT was negative in the patient with the TSH-secreting macroadenoma, and this tumor also showed no sensitivity to quinagolide in vivo or in vitro. 123I-IBZM is a ligand for in vivo imaging of dopamine agonist-sensitive macroprolactinomas, but not for microprolactinomas or GH-secreting adenomas. The technique potentially provides a means of predicting the dopamine agonist-responses of non-functioning pituitary adenomas in vivo.

Author (Year)	Title	Study Description	Number of Patients	Evidence Class	Conclusions
Luyken (1996)[81]	Clinical relevance of somatostatin receptor scintigraphy in patients with skull base tumours.	Patients with pituitary adenomas and other sellar/parasellar lesions underwent somatostatin receptor scintigraphy with octreotide. Results were compared between different groups of pathologies.	18	Diagnostic / III	All of the meningiomas (unifocal and multifocal tumors in various locations) showed a high density of SBS, whereas in none of the examined neurinomas SR were found. Pituitary adenomas revealed in only 50% SR in different concentrations and independent of the endocrine activity. A dural infiltration with meningioma tissue ("meningeal sign") may be discriminated from a reactive hypervascularisation in lesions with a diameter >0.5 cm. SRS can help in the differential diagnosis between meningiomas and other tumors, postoperative scar, or radionecrosis at the skull base.
Tumiati (1995)[82]	Scintigraphic assessment of pituitary adenomas and several diseases by indium-111-pentetreotide.	Clinical experience using indium-111-pentetreotide for the assessment of pituitary lesions.	21	Diagnostic/ III	In vivo scintigraphy showed pentetreotide receptors only in large GH-secreting adenomas and several macroadenomas. Concerning the endocrine activity of the adenomas, 111In-octreotide showed a good sensibility in detecting GH-secreting tumors.

Author (Year)	Title	Study Description	Number of Patients	Evidence Class	Conclusions
Boni (1995)[83]	[111In-DTPA-D-Phe]-octreotide scintigraphy in functioning and non-functioning pituitary adenomas.	Patients with non-functioning pituitary adenomas and secretory adenomas underwent [111In-DTPA-D-Phe]-ocretotide scintigraphy. Uptake levels were compared between the different groups of pathologies.	12	Diagnostic / III	Only 2/12 patients with non-functioning pituitary adenoma showed a positive scan while 12/13 with GH secretion and 2/2 TSH macroadenomas had positive scans. [111In-DTPA-D-Phe]-octreotide scintigraphy is a useful tool to confirm the presence of somatostatin receptors in selected patients with GH- and TSH-secreting pituitary adenoma. The role of [111In-DTPA-D-Phe]-octreotide scintigraphy in non-functioning pituitary tumors remains to be established, but it could be useful for octreotide treatment in patients who refuse surgery or who are poor surgical candidates.

Author (Year)	Title	Study Description	Number of Patients	Evidence Class	Conclusions
Duet (1994)[84]	Somatostatin receptor imaging in non-functioning pituitary adenomas: value of an uptake index.	Patients with nonfunctioning pituitary adenomas, GH-secreting adenomas, or no tumor underwent pituitary scintigraphy with somatostatin analog pentetreotidean. The accumulation of this analog was expressed as an activity radio between the uptake of radioactivity by the adenoma to that of normal brain tissue. Activity ratios were compared between the different groups of pathologies.	22	Diagnostic / III	In 15 out of the 17 patients with GH-secreting adenoma, an accumulation of the radioligand was shown. Median activity ratio was 3.8 (range 1-6.9; in 14 AR were greater than 2.2) and ARs were directly correlated (r = 0.54; *P* < .05) with the suppressibility of plasma GH levels by octreotide (OC) acute administration. In 2 patients who repeated scintigraphy during chronic OC treatment, AR values were reduced. In all the 22 patients with NFA, an accumulation of 111In-P at the pituitary level was observed, and median AR was 3.0 (range 1.5-20; in 14 greater than 2.2). In vitro autoradiography of surgical specimens in 6 NFA patients revealed SS-R in 4 cases with high scintigraphic AR and negative results in 2 cases with low AR. Scintiscan was repeated during chronic OC treatment in 5 patients with high score: AR decreased in 1 patient, increased in 3, and did not change in the other patient. No changes in tumor size were shown in any of these patients. A total of 8 patients (3 GH secreting and 5 NFA) had "normal" AR values. In acromegaly scintigraphy with 111In-P visualizes functioning pituitary SS-R coupled to intracellular events that control hormonal hypersecretion and tumor growth. In contrast, in spite of the positivity of 111In-P imaging in most patients with NFA, their receptors might have a defect in the coupling-transduction process, as they are not inhibited by OC treatment and no tumor shrinkage is observed.

Author (Year)	Title	Study Description	Number of Patients	Evidence Class	Conclusions
Colombo (1996)[85]	Three-step immunoscintigraphy with anti-chromogranin A monoclonal antibody in tumours of the pituitary region.	Patients with nonfunctioning pituitary adenomas and secretory adenomas underwent immunoscintigraphy with antichromogranin A monoclonal antibody and/or [111In]pentetreotide scintigraphy. Results were compared between the two modalities and the different groups of pathologies.	11	Diagnostic / III	Positive immunoscintigraphy with anti-chormogrnain A antibody was obtained in 9/11 (82%) non-functioning, but less in hormone-secreting adenomas. In conclusion, ISG is able to image pituitary tumors and particularly non-functioning pituitary adenomas. In this respect, it may be helpful in discriminating non-neuroendocrine masses of the pituitary region from non-functioning pituitary adenomas.
Kurtulmus (2007)[86]	The value of Tc-99m tetrofosmin in the imaging of pituitary adenomas.	Patients with and without pituitary adenomas underwent single-photon emission computed tomography (SPECT) imaging. Tc-99m uptake indices were compared statistically via Mann-Whitney U test between pituitary adenomas and normal controls.	15	Diagnostic / III	The average tetrofosmin uptake index of pituitary adenoma is 2.44+/-1.54 for the patients and 1.69+/-0.71 for the control group. Any significant difference was not observed between the groups (*P* = .3). The average index was calculated as 3.04+/-2.15 for invasive adenomas and 1.92+/-0.33 for the non-invasive group, and there was no significant difference between the 2 groups regarding uptake of the agent (P = .53). Furthermore, it was determined that the invasive and non-invasive adenomas displayed an uptake of Tc-99m TF similar to normal pituitary tissue. Since the pituitary adenoma and normal pituitary tissue gave similar results regarding Tc-99m TF uptake, it was concluded that this agent would not be useful in the diagnosis of pituitary adenoma.

Preoperative Imaging Characterization Evidence Tables

Table 7: Use of Preoperative Imaging to Differentiate NFPAs from Other Pathologies

Author (Year)	Title	Study Description	Number of Patients	Evidence Class	Conclusions
Amstutz (2006)[87]	Hypothalamic hamartomas: Correlation of MR imaging and spectroscopic findings with tumor glial content.	Correlate the MR imaging and proton MR spectroscopic properties of hypothalamic hamartomas with histopathologic findings.	14	Diagnostic / III	Tumors with markedly elevated mI/Cr demonstrated an increased glial component.
Freeman (2004)[88]	MR imaging and spectroscopic study of epileptogenic hypothalamic hamartomas.	Correlate the MR imaging and proton MR spectroscopic properties of hypothalamic hamartomas with histopathologic findings.	72	Diagnostic / III	MR imaging and spectroscopy suggest reduced neuronal density and relative gliosis in hypothalamic harmartomas compared with normal gray matter.

Author (Year)	Title	Study Description	Number of Patients	Evidence Class	Conclusions
Stadlbauer (2008)[89]	Proton magnetic resonance spectroscopy in pituitary macroadenomas: preliminary results.	Patients underwent proton MR (1H-MR) spectroscopy. Metabolite concentration of choline containing compounds was correlated to histological and surgical findings of hemorrhage as well as MIB-1 as a proliferative index.	16	Diagnostic / III	The study found a strong positive linear correlation between metabolite concentrations of Cho and the MIB-1 proliferative cell index (R = 0.819, *P* < .001). Eleven patients had a hemorrhagic adenoma and showed no assignable metabolite concentration of Cho, and the FWHM water was 13.4-24.4 Hz. In 10 patients, the size of the lesion was too small (<20 mm in 2 directions) for the acquisition of MR spectroscopy data. Quantitative 1H-MR spectroscopy provided important information on the proliferative potential and hemorrhaging of pituitary macroadenomas. These data may be useful for noninvasive structural monitoring of pituitary macroadenomas.
Sutton (1997)[91]	Proton spectroscopy of suprasellar tumors in pediatric patients.	Correlate the MR imaging and proton MR spectroscopic properties of suprasellar tumors.	19	Diagnostic / III	All craniopharyngiomas showed a dominant peak at 1 to 2 ppm, consistent with lactate or lipids, with trace amounts of other metabolites. This was confirmed using high-resolution spectroscopy. Chiasmatic gliomas showed a profile of choline, N-acetylaspartate, and creatine, and the choline:N-acetylaspartate ratio was 2.6 +/- 1.3, compared with 0.7 +/- 0.3 for samples of healthy brain (*t* test, *P* = .0003). Pituitary adenomas showed only a choline peak or no metabolites at all.
Sener (2001)[92]	Proton MR spectroscopy of craniopharyngiomas	Correlate the MR imaging and proton MR spectroscopic properties of craniopharyngiomas.	5	Diagnostic / III	Craniopharyngiomas display very prominent peaks centered at 1-1.5 ppm, which probably corresponded to lipid/cholesterol peaks.

Author (Year)	Title	Study Description	Number of Patients	Evidence Class	Conclusions
Faghih Jouibari (2012)[93]	Complementary effect of H MRS in diagnosis of suprasellar tumors.	Patients with suprasellar tumors underwent conventional MRI and magnetic resonance spectroscopy. A radiologist recorded the most probable diagnosis using only conventional MR imaging and then conventional MR imaging with magnetic resonance spectroscopy. These diagnoses using either a single or both modalities were compared to a pathology report as the gold standard.	23	Diagnostic / III	The information provided by MRS led the radiologist to alter his prior diagnosis that was based on the MRI in 4 patients, and the final diagnoses were in accordance with the histopathology. Wrong diagnosis was made by MRI plus MRS in 3 patients. Test efficiency of MRI was 69.6%, and it was 87% for MRI plus MRS. However, the difference was not statistically significant (*P*= .152). MRS may be useful in providing a more improved preoperative diagnosis of suprasellar tumors when used in addition to MRI.

Author (Year)	Title	Study Description	Number of Patients	Evidence Class	Conclusions
Bladowska (2013)[60]	Usefulness of perfusion weighted magnetic resonance imaging with signal-intensity curves analysis in the differential diagnosis of sellar and parasellar tumors: preliminary report.	Patients underwent both conventional MRI and perfusion weighted MR imaging. Mean and maximum values of relative cerebral blood volume, relative peak height, and relative percentage of signal intensity recovery were calculated from the perfusion weighted MR images. These parameters were compared between different pathologies (pituitary macroadenomas, meningiomas, craniopharyngioma, hemangioblastoma, glioma, and metastasis).	23	Diagnostic / III	There were statistically significant differences in the mean and maximum rCBV values (P = .026 and P = 0.019, respectively). The maximum rCBV values >7.14 and the mean rCBV values >5.74 with the typical perfusion curve were very suggestive of the diagnosis of meningioma. Perfusion weighted MR imaging can provide supplemental information to differentiate pituitary adenomas from meningiomas. However, it is unclear how this improves the sensitivity and specificity of diagnosis of sellar/parasellar tumors.
Yamamura (2003)[74]	Differentiation of pituitary adenomas from other sellar and parasellar tumors by 99mTc(V)-DMSA scintigraphy.	Patients with pituitary adenomas and other sellar/parasellar lesions underwent pentavalent technetium-99m dimercaptosuccinic acid scintigraphy. Imaging findings were compared by differing pathology.	21	Diagnostic / III	99mTc(V)-DMSA scintigraphy showed overall sensitivity of 81% (17/21 cases) for detecting pituitary adenomas, in particular 100% for non-functioning adenomas. 99mTc(V)-DMSA may be useful for detecting pituitary adenomas, especially non-functioning adenomas, and for the differentiation of non-functioning pituitary adenomas from other sellar and parasellar lesions.

Author (Year)	Title	Study Description	Number of Patients	Evidence Class	Conclusions
Lastoria (1995)[75]	Technetium-99m pentavalent dimercaptosuccinic acid imaging in patients with pituitary adenomas.	Patients with nonfunctioning pituitary adenomas, secretory adenomas, or non-tumor controls underwent technetium-99m-labeled pentavalent dimercaptosuccinic acid scintigraphy. Uptake levels were compared between the different groups of pathologies.	15	Diagnostic / III	Seventeen GH-secreting (81%), 7 PRL-secreting (78%), 3 ACTH-secreting (50%), 15 non-functioning (100%), and 1 (50%) mixed adenoma significantly concentrated [99mTc](V)DMSA, showing elevated tumor-to-background (T/B) ratios. Non-adenomatous lesions of the sella turcica did not concentrate [99mTc](V)DMSA in the pituitary as well as brain tumors and 8 out of 10 metastatic thyroid cancers. The [99mTc](V)DMSA scintigraphy showed an overall sensitivity of 81% (43/53) in detecting pituitary adenomas, which was increased to 95% for lesions greater than 10 mm in size. High-quality images with minimal total body radiation were obtained, enabling a good in vivo characterization of viable adenomatous tissue as well as an accurate monitoring of the effects of different therapeutic regimens. Technetium-99m DMSA may be used as a supplementary tool in the preoperative identification of pituitary adenoma.

Author (Year)	Title	Study Description	Number of Patients	Evidence Class	Conclusions
Kobayashi (1994)[94]	A clinical and histopathological study of factors affecting MRI signal intensities of pituitary adenomas.	Conventional MR imaging of patients with nonfunctioning pituitary adenomas and secretory adenomas were retrospectively reviewed. MR signal intensities were calculated from the T1-weighted images and compared between the groups of different pathologies. Immunohistochemical staining allowed for calculation of the proportion of hormone positive cells. Age, maximal diameter of the tumor, cell density, and the proportion of hormone-positive cells were placed in a multiple regression analysis using signal intensity as the dependent variable.	18	Diagnostic / III	Four independent variables were used in the analysis: the age of the patient, the maximum diameter of the adenoma, the cell density, and the proportion of hormone-positive cells in the adenoma. With the signal intensity ratio as the dependent variable, a multiple regression analysis was performed. The great influence upon the signal intensities on T1-weighted images was the proportion of hormone-positive cells. This suggests signal intensities on T1W images may help with prediction of functioning versus NFPAs

Author (Year)	Title	Study Description	Number of Patients	Evidence Class	Conclusions
Spiller (1997)[95]	Secretory and nonsecretory pituitary adenomas are distinguishable by 1/T1 magnetic relaxation rates at very low magnetic fields in vitro.	Clinical experience using 1/T1 magnetic relaxation to discriminate between secretory and nonsecretory pituitary adenomas.	18	Diagnostic / III	Mean 1/T1 was significantly higher ($P < .02$) for hormone-secreting than for nonsecreting adenomas at fields below 0.24 T; no significant difference existed at typical MR imaging fields (0.5 to 1.5 T). Mean 1/T1 for hormone-producing and nonhormone-producing, nonsecreting adenomas were not significantly different at any field. Because 1/T1 at low fields is related to 1/T2 at imaging fields, it may be possible to detect hormone secretion of pituitary adenomas noninvasively by MR imaging.
Zada (2010)[96]	Patterns of extrasellar extension in growth hormone-secreting and nonfunctional pituitary macroadenomas.	Patients with histologically confirmed nonfunctional pituitary macroadenomas or GH secreting macroadenomas and pre-operative MR imaging had MR imaging evaluated in terms of mean maximal tumor diameter and patterns of extrasellar extension. These were compared between the two subtypes studied.	50	Diagnostic / III	The mean maximal tumor diameter in NFMAs and GH-secreting macroadenomas was 26 and 16 mm, respectively ($P < .0001$). Compared with GH-adenomas, NFMAs were more likely to develop suprasellar extension (82% vs 16%, $P < .0001$), cavernous sinus extension (40% vs 16%, $P = .04$), and isolated suprasellar extension (30% vs 4%, $P = .0145$). GH-macroadenomas had higher overall rates of infrasellar extension (72% vs 46%, $P < .05$) and isolated infrasellar extension (52% vs 6%, $P < .0001$). Substantial differences in extrasellar growth patterns were observed among varying histological subtypes of pituitary macroadenomas. Despite smaller tumor diameters, GH-macroadenomas demonstrated a proclivity for infrasellar extension, whereas NFMAs exhibited preferential extension into the suprasellar region.

Author (Year)	Title	Study Description	Number of Patients	Evidence Class	Conclusions
Luo (2000)[97]	Imaging of invasiveness of pituitary adenomas.	CT and/or MR imaging of patients with pituitary tumors were retrospectively reviewed. The images were assessed for tumor size, extension, and direction of tumor spread.	135	Diagnostic / III	One hundred and seventeen patients (87%) had suprasellar extension with compression of optic apparatuses, and 12 patients (9%) had extension of tumor upward to hypothalamus and third ventricle. Infrasellar extension via the floor of the sella and sphenoid sinus was found in 38 patients (28%), and further downward extension to ethmoid sinus, nasopharynx, and/or skull base was depicted in 5 patients (4%). Twenty-two patients (16%) had lateral invasion to the cavernous sinus and associated cranial nerves. Temporal and frontal extensions were depicted in 7 patients (5%) and 6 patients (4%), respectively. Five patients (4%) had posterior subtentorial extension to posterior fossa. Histologically, only 2 patients showed microscopic invasive features. There was no correlation between histologic features and imaging invasiveness. Pituitary adenomas have the potential of multi-directional extension. This experience indicated any type of pituitary adenoma could invade surrounding structures. Suprasellar invasion was the most common direction of pituitary adenoma spread, followed by infrasellar, lateral, anterior, and posterior routes.

Author (Year)	Title	Study Description	Number of Patients	Evidence Class	Conclusions
Lundin (1992)[98]	MRI of pituitary macroadenomas with reference to hormonal activity.	Patients with nonfunctioning pituitary adenomas and secretory adenomas underwent conventional MR imaging. Signal intensity patterns, relaxation times, and ratios of signal intensity and proton density relative to the corpus callosum were calculated and compared between the different groups of pathologies.	64	Diagnostic / III	Invasiveness was more common in PRL- and GH-secreting adenomas than in the nonsecreting ones. Diffuse invasion of the base of the skull was most common in prolactinomas and associated with a lower frequency of suprasellar tumor extension. In prolactinomas, a correlation was found between the maximum serum PRL level and tumor size. Hemorrhagic, cystic, or necrotic areas were less common in GH-secreting tumors than in the other types. Hemorrhage was more common in prolactinomas than in nonsecreting tumors. MR parameters were similar in prolactinomas and nonsecreting adenomas but indicated a smaller amount of water in GH-secreting tumors. MR parameters may be used to identify histology of different pituitary adenomas.

Author (Year)	Title	Study Description	Number of Patients	Evidence Class	Conclusions
Chang (2000)[99]	Computed tomography and magnetic resonance imaging characteristics of giant pituitary adenomas.	CT and/or MR imaging of patients with pituitary tumor were retrospectively reviewed. The tumor appearances and patterns of extension were recorded.	14	Diagnostic / III	Thirteen tumors (93%) extended upward to the suprasellar cistern and/or hypothalamus and third ventricle. Infrasellar extension through the sellar floor and sphenoid sinus to the skull base, or to the ethmoid sinus or the nasopharynx, was identified in 7 patients (50%). Eight patients (57%) had lateral invasion to the cavernous sinus. Temporal and frontal extension was apparent in 7 patients (50%) and 6 patients (43%), respectively. Five patients (36%) had posterior subtentorial extension to the posterior fossa. Histologically, only 2 GPAs showed invasive features. There was no correlation among histologic features, pituitary hormone concentrations, and evidence of tumor aggressiveness on CT and MRI scans. Any type of pituitary adenoma, regardless of its endocrinologic activity, may invade surrounding structures. Suprasellar invasion is the most common pathway of tumor spread, followed by infrasellar, lateral, anterior, and posterior routes.

Author (Year)	Title	Study Description	Number of Patients	Evidence Class	Conclusions
Cazabat (2014)[100]	Silent, but not unseen: multimicrocystic aspect on T2-weighted MRI in silent corticotroph adenomas.	Preoperative T2-weighted MR images were retrospectively evaluated in patients with histologically proven (1) silent corticotroph adenomas, (2) corticotroph macroadenomas, and (3) nonfunctional gonadotroph macroadenomas by a single radiologist blind to histologic/clinical diagnosis.	77	Diagnostic / III	Multiple microcysts were present in 76% (13/17) of SCAs, 21% (3/14) of CSMs, and 5% (3/60) of NFGMs. The presence of MMs in clinically nonfunctioning macroadenomas had a sensitivity of 76% and a specificity of 95% for predicting SCA. The presence of MMs in T2-weighted MRI is a potential diagnostic tool to suggest the histologic subtype in NFPAs.
Nishioka (2012)[101]	Correlation between histological subtypes and MRI findings in clinically nonfunctioning pituitary adenomas.	Patients with conventional MR imaging and classification of histological subtype of nonfunctioning pituitary adenomas were retrospectively analyzed. MR findings were correlated to different histological subtypes as well as MIB-1 index and patient age.	390	Diagnostic / III	Three MRI findings were less common in NCA/SGA than in the other groups ($P < .0001$): giant adenoma (>40 mm), marked cavernous sinus invasion (Knosp grade 4), and lobulated configuration of the suprasellar tumor. When these MRI findings were negative in patients older than 40 years old, 91.0% (212/233) were NCA/SGA. NFPA subtypes including silent corticotroph and other silent adenomas are associated with certain radiologic signs.

Table 8: Cavernous Sinus Wall Invasion

Author (Year)	Title	Study Description	Number of Patients	Evidence Class	Conclusions
Pan (2005)[102]	Magnetic resonance imaging and biological markers in pituitary adenomas with invasion of the cavernous sinus space.	Patients with conventional MRI were prospectively analyzed for cavernous sinus invasion and compared to intraoperative findings as the gold standard. Tumors with invasion were compared to tumors without invasion in terms of F8-related antigen, Ki-67 LI, VEGF, MMP-9, c-myc, bcl2, and nm23.	45	Diagnostic / II	The sensitivity of MRI for indicating cavernous sinus invasion in this prospective study was 60%, specificity 85%, positive predictive value 83.33%, negative predictive value 62.96%. The results have shown that MVD of invasive pituitary adenomas was significantly higher than that of noninvasive ($P < .001$). There was an association between the invasion of pituitary adenomas and Ki-67 LI ($P = .039$) or the expression of VEGF ($P < .001$) and MMP-9 ($P < .001$). Parasellar extension of pituitary adenomas through the medial wall of the cavernous sinus diagnosed at surgery, can be determined by radiology with sensitive gadolinium-enhanced MRI. VEGF, Ki-67, nm23, and MMP-9 have associations with invasiveness of pituitary adenomas, but lack specificity.

Author (Year)	Title	Study Description	Number of Patients	Evidence Class	Conclusions
Connor (2014)[103]	Magnetic resonance imaging criteria to predict complete excision of parasellar pituitary macroadenoma on postoperative imaging.	Preoperative and matched 3-month postoperative MR images were compared in patients with pituitary macroadenomas with parasellar involvement. Specifically, 12 preoperative MRI findings were compared to the presence or absence of postoperative evidence of complete resection.	49	Diagnostic / III	Depiction of the inferolateral (positive predictive value [PPV]: 0.6; negative predictive value [NPV], 0.92) and lateral (PPV: 0.65; NPV: 0.85) compartments of the cavernous sinus and the percentage of intracavernous carotid artery encasement (PPV: 0.63; NPV, 1.0 for <50% encasement) were significantly predictive of complete resection. The odds ratios indicated that depiction of the lateral venous or inferolateral venous compartments increased the likelihood of a complete resection by 6 times, whereas for every 25% reduction in intracavernous carotid artery encasement, the chance of a complete resection increased 3.4 times. Two preoperative MRI features (depiction of the lateral and inferolateral compartment of the cavernous sinus and decreasing encasement of the intracavernous carotid artery) may be useful in predicting total resection of parasellar components of pituitary adenomas.
Daniels (1988)[104]	MR imaging of the cavernous sinus: value of spin echo and gradient recalled echo images.	Clinical experience examining the utility of spin echo gradient recalled echo images in assessing the anatomy of the cavernous sinus.	25	Diagnostic / III	Correlation of coronal T1-weighted spin echo and gradient recalled echo images (the latter with high-signal-intensity vascular structures) proved to be an effective means of identifying cavernous venous spaces, connective tissue and cranial nerves, and the lateral margins of the pituitary gland, and of differentiating tumor tissue from cavernous venous spaces.

Author (Year)	Title	Study Description	Number of Patients	Evidence Class	Conclusions
Ahmadi (1986)[105]	Cavernous sinus invasion by pituitary adenomas.	Clinical experience using CT to assess pituitary lesions with cavernous sinus invasion.	19	Diagnostic / III	CT findings included cavernous sinus expansion (17 patients) and visible encasement of the internal carotid artery (14 patients). The invasive tumor often enhanced to a lesser degree than the cavernous sinuses and ipsilateral internal carotid artery. Intracavernous cranial nerve compression, obliteration, or displacement (14 patients), invasion of the lateral wall of the cavernous sinus (7 patients), and diffuse bone destruction (7 cases) were other findings. Magnetic resonance imaging in 3 patients provided excellent demonstration of intracavernous internal carotid artery encasement, but displacement and obliteration of intracavernous cranial nerves was not shown as well as it was with CT. There was no correlation between histologic features, hormone assays, and invasiveness. This experience indicates any type of pituitary adenoma, regardless of its endocrinologic activity, can invade the cavernous sinus.

Author (Year)	Title	Study Description	Number of Patients	Evidence Class	Conclusions
Davis (2013)[51]	Evaluation of the pituitary gland using magnetic resonance imaging: T1-weighted vs VIBE imaging.	Patients underwent both coronal T1-weighted and volumetric interpolated breath-hold examination imaging (VIBE). The 2 sequences were compared in terms of contrast enhancement, cavernous sinus appearance, and optic chiasm appearance. For each subject, VIBE was rated as better, equal, or worse to T1-weighted images and statistically compared using chi-square tests. These comparisons were also made while stratifying for macroadenomas and post-surgical patients.	32	Diagnostic / III	There was a trend to VIBE being superior to T1W for visualization of pituitary adenomas, but these data were not statistically significant. Visualization of chiasm in macroadenomas was similar for both techniques. VIBE was significantly superior to T1W with respect to pituitary and cavernous sinus contrast enhancement and cavernous sinus anatomy. Although not statistically significant, VIBE may improve the resolution of MR images for pre-operative visualization of pituitary adenomas, cavernous sinus invasion, and optic chiasm compression. This strength may be even larger with higher tesla magnets.

Author (Year)	Title	Study Description	Number of Patients	Evidence Class	Conclusions
Cukiert (1998)[106]	Cavernous sinus invasion by pituitary macroadenomas. Neuroradiological, clinical, and surgical correlation.	Preoperative MR images of patients with and without intraoperative confirmation of cavernous sinus invasion were retrospectively studied. MR signs such as tumor lateral to the carotid artery, tumor within the carotid syphon, and lack of ring enhancement of the medial wall of the cavernous sinus were evaluated in the 2 groups of patients.	18	Diagnostic / III	Only 8 patients had tumor lateral to the carotid artery, 13 had tumor within the carotid syphon, and all lacked the ring enhancement of the medial wall of the cavernous sinus. In 10 patients, widening of the posterior double leaflets of the cavernous sinus could be seen. Only 3 patients disclosing the above-mentioned MRI features were identified in a series of 250 patients and did not have cavernous sinus invasion. The present criteria proved to be useful in the preoperative diagnosis of cavernous sinus invasion and patients' counselling.
Knosp (1991)[107]	Pituitary adenomas with parasellar invasion.	MR imaging of pituitary adenomas with surgically confirmed invasion into the cavernous sinus were retrospectively evaluated. MR signs were correlated to cavernous sinus invasion using surgical experience as the gold standard. Cavernous sinus invasion was also correlated with KI-67 measurements.	25	Diagnostic / III	When the adenoma encases the intracavernous internal carotid artery or reaches as far as to the lateral aspect of the artery, invasion was present in all cases. The critical area where invasion could not be predicted from MRI is the distance between the medial and the lateral aspect of the intracavernous internal carotid artery. By measurement with the monoclonal antibody KI-67, it could be shown that pituitary adenomas infiltrating the parasellar space have a statistically significant higher growth rate (*P* less than .001), compared to non-invasive adenomas. These criteria can potentially be used to identify cavernous sinus invasion.

Author (Year)	Title	Study Description	Number of Patients	Evidence Class	Conclusions
Knosp (1993)[108]	Pituitary adenomas with invasion of the cavernous sinus space: a magnetic resonance imaging classification compared with surgical findings.	MR imaging of pituitary adenomas with surgical confirmation of invasion into the cavernous sinus space were retrospectively evaluated. Images were classified by grade 0-4 using the internal carotid artery as a radiologic landmark.	12	Diagnostic / III	Grades 0, 1, 2, and 3 are distinguished from each other by a medial tangent, the intercarotid line—through the cross-sectional centers—and a lateral tangent on the intra- and supracavernous internal carotid arteries. Grade 0 represents the normal condition, and Grade 4 corresponds to the total encasement of the intracavernous carotid artery. According to this classification, surgically proven invasion of the cavernous sinus space was present in all Grade 4 and Grade 3 cases and in all but 1 of the Grade 2 cases; no invasion was present in Grade 0 and Grade 1 cases. Therefore, the critical area where invasion of the cavernous sinus space becomes very likely and can be proven surgically is located between the intercarotid line and the lateral tangent, which is represented by our Grade 2. The monoclonal antibody KI-67 showed a statistically higher proliferation rate ($P < .001$) in adenomas with surgically observed invasion into the cavernous sinus space, as compared with noninvasive adenomas. The Knosp criteria, specifically the differentiation of grades 1/2 vs 3/4, can be used to characterize cavernous sinus invasion preoperatively.

Author (Year)	Title	Study Description	Number of Patients	Evidence Class	Conclusions
Scotti (1988)[109]	MR imaging of cavernous sinus involvement by pituitary adenomas.	Clinical experience using MR to assess macroadenomas with and without cavernous sinus involvement.	11	Diagnostic / III	In 10 of the 11 macroadenomas with surgically proved dural invasion, MR demonstrated an asymmetric increase in size and intensity of the superior and inferior cavernous sinus compartments. Noninvasive macroadenomas compressed and displaced the cavernous sinus bilaterally. The prospective MR evaluation of 30 patients undergoing surgery for pituitary tumor revealed a sensitivity for predicting cavernous sinus invasion of 55%, a specificity of 85.7%, a positive predictive value of 62.5%, and a negative predictive value of 81.8%. No feature permitted certain distinction between invasive and noninvasive microadenomas, as the medial dural wall of the cavernous sinus could not be reliably identified. MR parameters can identify cavernous sinus invasion, with the most specific sign of cavernous sinus invasion being carotid artery encasement.

Author (Year)	Title	Study Description	Number of Patients	Evidence Class	Conclusions
Sol (2014)[110]	Evaluation of MRI criteria for cavernous sinus invasion in pituitary macroadenoma.	Coronal T2-weighted MR images of patients with pituitary adenoma with cavernous sinus invasion were retrospectively evaluated. The MR signs assessed were: presence of hypointense line suggestive of medial wall of cavernous sinus, presence of entire rim-enhancement around the intracavernous internal carotid artery, location of the tumor in relation to the lateral intercarotid lines, and angle of the tumor encasement around the intracavernous ICA. These signs were analyzed using intraoperative findings as the gold standard.	63	Diagnostic / III	CS invasion was highly probable if periarterial enhancement was not depicted (positive predictive value, 86%; $P < .001$). Valuable criteria of CS invasion by logistic regression analysis were the absence of periarterial enhancement ($P = .043$, odds ratio = 5.23) and the angle of intracavernous ICA encased by the tumor ($P = .029$, odds ratio = 1.017), with a threshold value of 136.5° with a sensitivity of 90% and specificity of 78.3%. The MRI criteria described in this study can be useful in evaluating CS invasion in pituitary adenomas.

Author (Year)	Title	Study Description	Number of Patients	Evidence Class	Conclusions
Vieira (2006)[112]	Evaluation of magnetic resonance imaging criteria for cavernous sinus invasion in patients with pituitary adenomas: logistic regression analysis and correlation with surgical findings.	Patients with pituitary adenomas with or without cavernous sinus invasion and conventional MR imaging were retrospectively evaluated. MR imaging findings included: presence of normal pituitary gland between the adenoma and cavernous sinus, status of the cavernous sinus venous compartments, cavernous sinus size, cavernous sinus lateral wall bulging, displacement of the intracavernous internal carotid artery by adenoma, Knosp-Steiner criteria, and percentage of intracavernous internal carotid artery encased by the tumor. These findings were compared to surgical description as the gold standard.	103	Diagnostic / III	The following signs were found to represent accurate criteria for noninvasion of the CS: (1) normal pituitary gland interposed between the adenoma and the CS (PPV, 100.0%), (2) intact medial venous compartment (PPV, 100.0%), and (3) percentage of encasement of the intracavernous ICA lower than 25% (NPV, 100.0%). Cavernous sinus invasion was certain if the percentage of encasement of the intracavernous ICA was higher than 45% and 3 or more CS venous compartments were not depicted. The most valuable criterion of CSI by logistic regression analysis was the percentage of encasement of intracavernous ICA of 30% or more, with an odds ratio of 49.25. The preoperative diagnosis of CSI by PA is extremely important because endocrinologic remission is rarely obtained after microsurgery alone in patients with invasive tumors. The evaluated MR imaging criteria may be useful in patient management and in advising most of the patients preoperatively on the potential need for complimentary therapy after surgery.

Author (Year)	Title	Study Description	Number of Patients	Evidence Class	Conclusions
Vieira (2004)[113]	Magnetic resonance imaging of cavernous sinus invasion by pituitary adenoma diagnostic criteria and surgical findings.	Conventional MR imaging of patients with and without cavernous sinus invasion were retrospectively reviewed. MR signs including presence of normal pituitary gland between the adenoma and cavernous sinus, status of the cavernous sinus venous compartments, cavernous sinus size, cavernous sinus lateral wall bulging, displacement of the intracavernous internal carotid artery by adenoma, grade of parasellar extension, and percentage of intracavernous internal carotid artery encased by tumor were assessed. These were compared using chi squared tests to intraoperative findings as the gold standard.	103	Diagnostic / III	The following signs have been found to represent accurate criteria for non-invasion of the CS: 1, normal pituitary gland interposed between the adenoma and the CS (PPV, 100%); 2, intact medial venous compartment (PPV, 100%); 3, percentage of encasement of the intracavernous ICA lower than 25% (NPV, 100%); and 4, medial intercarotid line not crossed by the tumor (NPV, 100%). Criteria for CSI were: 1, percentage of encasement of the intracavernous ICA higher than 45%; 2, occlusion of 3 or more CS venous compartments; and 3, occlusion of the CS lateral venous compartment. The CS was very likely to be invaded if the inferior venous compartment was not detected (PPV, 92.8%), if the lateral intercarotid line was crossed (PPV, 96.1%), or if a bulging lateral dural wall of the CS was seen (PPV, 92.3%). The above-mentioned MR imaging criteria may be useful in advising most of the patients preoperatively on the potential need for complimentary therapy after surgery.

Author (Year)	Title	Study Description	Number of Patients	Evidence Class	Conclusions
Cottier (2000)[114]	Cavernous sinus invasion by pituitary adenoma: MR imaging.	Patients with conventional MR imaging were retrospectively reviewed. Nine MRI signs of cavernous sinus invasion were assessed on preoperative images. These signs were compared with chi squared tests using surgical findings as the gold standard.	106	Diagnostic / III	Invasion of the cavernous sinus was certain (PPV, 100%) if the percentage of encasement of the internal carotid artery (ICA) by tumor was 67% or greater. It was highly probable if the carotid sulcus venous compartment was not depicted (PPV, 95%) or the line joining the lateral wall of the intracavernous and supracavernous ICAs was passed by the tumor (PPV, 85%). It was definitely not invaded (NPV, 100%) if the percentage of encasement of the intracavernous ICA was lower than 25% or the line joining the medial wall of the intracavernous and supracavernous ICAs was not passed by the tumor. The radiologic diagnosis of cavernous sinus invasion by pituitary adenoma can be aided by the criteria in this study.

Author (Year)	Title	Study Description	Number of Patients	Evidence Class	Conclusions
Steiner (1994)[40]	MR-appearance of the pituitary gland before and after resection of pituitary macroadenomas.	Clinical experience using MR to assess pituitary macroadenomas prior to and after surgical excision.	30	Diagnostic / III	On preoperative MR images, contrast administration increased the detectability of the anterior lobe from 30% to 80%. Depending on the size and extension of the adenoma, the pituitary gland was displaced to the suprasellar space (53%) and/or deformed to a club-shaped (27%) or sickle-shaped (47%) configuration. In 6 patients, the sickle-shaped pituitary gland was interposed between the cavernous sinus and the adenoma ("rim-sign"), which was seen only on gadopentetate dimeglumine-enhanced images. In these cases, there was no infiltration of the cavernous sinus at surgery. Postoperatively, descent of the pituitary gland was found in 63%, and re-expansion in 54%. We conclude that contrast administration improves the detectability of the pituitary gland on preoperative MR images, and that the displacement and deformation of the pituitary gland depend on the size, location, and extension of the adenoma. Preoperatively, demonstration of the pituitary gland interposed between the cavernous sinus and the adenoma ("rim-sign") is a very useful sign for exclusion of cavernous sinus infiltration, best seen on contrast-enhanced coronal MR images.

Author (Year)	Title	Study Description	Number of Patients	Evidence Class	Conclusions
Daita (1995)[115]	Cavernous sinus invasion by pituitary adenomas—relationship between magnetic resonance imaging findings and histologically verified dural invasion.	Clinical experience using MR to assess pituitary lesions with dural invasion.	26	Diagnostic / III	All patients were classified according to MR imaging findings into 3 types. Type I showed a gadolinium-enhanced stripe medial to the carotid artery (5 patients), none of which showed dural invasion. Type II showed no enhanced stripe (17 patients), 6 of which showed dural invasion. Within this type, tumor size and dural invasion showed no correlation. Type III showed displacement or encasement of the carotid artery by the tumor with or without extracranial extension (4 patients), all of which showed massive infiltration of the tumor cells into the dura mater. This study shows that preoperative MR imaging can provide information for assessment of invasion into the cavernous sinus in patients with pituitary adenoma.
Nakasu (2001)[116]	Tentorial enhancement on MR images is a sign of cavernous sinus involvement in patients with sellar tumors.	Patients with pituitary adenomas and other sellar/parasellar lesions underwent conventional MR imaging. Enhancement patterns of the dura around the tumors were compared with levels of tumor invasion or compression of the cavernous sinus, where intraoperative experience was the gold standard.	64	Diagnostic / III	For evaluation of cavernous sinus invasion ipsilateral to the enhancement, sensitivity and specificity of the asymmetric tentorial enhancement sign were 81.3% and 86.3%, respectively. Sensitivity and specificity of the sign were 42.9% and 93.6% for cavernous sinus involvement, including compression and invasion. Asymmetric tentorial enhancement is a useful sign in the diagnosis of invasion or severe compression of the cavernous sinus by sellar tumor. The sign may represent venous congestion or collateral flow in the tentorium due to obstructed flow in the medial portion of the cavernous sinus.

Author (Year)	Title	Study Description	Number of Patients	Evidence Class	Conclusions
Cattin (2000)[117]	Dural enhancement in pituitary macroadenomas.	Patients with and without pituitary adenomas underwent conventional MR imaging. Dural enhancement patterns of the sellar region were analyzed and noted if abnormal. Differences in dural enhancement patterns between the 2 groups were compared.	20	Diagnostic / III	Dural enhancement appeared to be usually abnormal in 20 patients with pituitary macroadenoma compared with 20 control patients, mainly at the planum sphenoidale and carotid sulcus. However, dural changes are subtle and their recognition requires knowledge of the normal enhancement patterns. Dural changes may also be seen in pituitary macroadenomas, although this is not a specific finding.
Nishioka (2012)[101]	Correlation between histological subtypes and MRI findings in clinically nonfunctioning pituitary adenomas.	Patients with conventional MR imaging and classification of histological subtype of nonfunctioning pituitary adenomas were retrospectively analyzed. MR findings were correlated to different histological subtypes as well as MIB-1 index and patient age.	390	Diagnostic / III	Three MRI findings were less common in NCA/SGA than in the other groups ($P < .0001$): giant adenoma (>40 mm), marked cavernous sinus invasion (Knosp grade 4), and lobulated configuration of the suprasellar tumor. When these MRI findings were negative in patients older than 40 years old, 91.0% (212/233) were NCA/SGA. NFPA subtypes including silent corticotroph, and other silent adenomas are associated with certain radiologic signs.

Author (Year)	Title	Study Description	Number of Patients	Evidence Class	Conclusions
Kunishio (2006)[118]	Technetium-99m sestamibi single photon emission computed tomography findings correlated with P-glycoprotein expression in pituitary adenoma.	Patients underwent technetium-99m sestamibi single photon emission computed tomography (SPECT). SPECT characteristics were compared to cavernous sinus invasion, proliferative potential, and multidrug resistance gene product P-glycoprotein expression.	10	Diagnostic / III	The pituitary adenomas specimens were examined by immunohistochemistry using anti-Pgp and MIB-1 monoclonal antibodies. (99m)Tc-MIBI SPECT findings were not related to MIB-1 labeling index or cavernous sinus invasion. (99m)Tc-MIBI SPECT RI (-38.55+/-20.77) of the Pgp-positive group was significantly lower than that (-15.78+/-19.40) of Pgp-negative group *(P* = .0494). No significant difference was observed in the ER and DR of (99m)Tc-MIBI SPECT between Pgp-positive and negative groups. This study suggests that although (99m)Tc-MIBI SPECT is not useful to evaluate the proliferative potential or cavernous sinus invasion of pituitary adenomas. (99m)Tc-MIBI SPECT could predict anti-cancer drug resistance related to the expression of Pgp in pituitary adenomas.
Nakano (2001)[119]	Use of 201Tl SPECT for evaluation of biologic behavior in pituitary adenomas.	Patients with pituitary adenomas underwent 201 Tl chloride SPECT studies. 201 Tl uptake indices were calculated, and these data were compared between invasive and noninvasive pituitary adenomas as well as monoclonal antibody labeling index.	22	Diagnostic / III	In comparison with noninvasive pituitary adenomas, invasive pituitary adenomas exhibited significantly higher 201Tl uptake indices on both the early and the delayed images (*P* = .0010 and .0019, respectively). A significant correlation was found between the 201Tl uptake index on the delayed image and the MIB1 labeling index (*P* = .0107). 201Tl SPECT can be useful for detecting biologic aggressiveness in pituitary adenomas.

Table 9: Vascularity and Hemorrhage

Author (Year)	Title	Study Description	Number of Patients	Evidence Class	Conclusions
Di Ieva (2007)[120]	Fractal dimension as a quantitator of the microvasculature of normal and adenomatous pituitary tissue.	Clinical experience characterizing vascular surface fractal dimension in pituitary lesions	34	Diagnostic / III	There was a statistical significant difference between the mean vascular surface fractal dimension estimated in normal vs adenomatous tissues (*P* = .01), normal vs secreting adenomatous tissues (*P* = .0003), and normal versus non-secreting adenomatous tissues (*P* = .047), whereas the difference between the secreting and non-secreting adenomatous tissues was not statistically significant. This demonstrates that fractal dimension is an objective and valid quantitator of the two-dimensional geometrical complexity of the pituitary gland microvascular network in physiological and pathological states.
Finelli (1993)[121]	Varied microcirculation of pituitary adenomas at rapid, dynamic, contrast-enhanced MR imaging.	Patients with pituitary adenomas underwent dynamic contrast enhanced MR imaging. The early enhancement patterns of normal pituitary structures and tumor tissue was documented.	16	Diagnostic / III	Arterial-phase enhancement of 16 macroadenomas was observed, suggesting a primary arterial blood supply to these lesions. The technique reveals the microcirculatory dynamics associated with pituitary adenomas and suggests a dominant arterial blood supply for macroadenomas. Arterial phase enhancement can be used to characterize microcirculation for preoperative assessment and surgical planning.

Author (Year)	Title	Study Description	Number of Patients	Evidence Class	Conclusions
Yuh (1994)[123]	Sequential MR enhancement pattern in normal pituitary gland and in pituitary adenoma.	Patients with pituitary adenomas and non-tumor controls prospectively underwent dynamic MR imaging with either a 5 or 10 second temporal resolution during a bolus injection of gadolinium. Qualitative visual analysis of the enhancement patterns via the MR images were compared between the 2 groups of patients.	10	Diagnostic / II	Quantitative analysis revealed that posterior lobe enhancement occurred 9.8 +/- 1.5 sec (mean +/- SEM) before the anterior lobe in healthy subjects, whereas tumor enhancement occurred significantly before the anterior lobe but only slightly before the posterior lobe in patients with adenomas. The sequential enhancement pattern of the normal pituitary gland was found to be consistent with its vascular anatomy. In contrast to previous reports, pituitary adenomas were found to enhance earlier than the anterior lobe. These results suggest that pituitary adenomas have a different MR enhancement pattern from normal tissue and may be because of a direct arterial blood supply, similar to that of the posterior pituitary lobe.

Author (Year)	Title	Study Description	Number of Patients	Evidence Class	Conclusions
Sakai (2013)[62]	Arterial spin-labeled perfusion imaging reflects vascular density in nonfunctioning pituitary macroadenomas.	Patients underwent both conventional MR imaging and arterial spin-labeled perfusion imaging. Degree of enhancement was calculated by dividing the signal intensity on T1-weighted with contrast to the T1-weighted without contrast. Normalized tumor blood flow values were calculated by dividing the mean value of the tumor region of interest by mean region of interest values in the cerebellar hemispheres. Relative microvessel attenuation was calculated by dividing the total microvessel wall area by entire CD31 stained tissue area. These parameters were compared with each other as well as the presence of intra- or postoperative hemorrhage by surgeon visualization.	11	Diagnostic / III	A statistically significant difference in normalized tumor blood flow values was observed visually between the intraoperative hypovascular and hypervascular groups ($P < .05$). One of these hypervascular cases actually did have symptomatic postoperative hemorrhage. ASL perfusion imaging can reflect the vascular density of NFPAs and may be a viable test in predicting intra/postoperative tumor hemorrhage.

Author (Year)	Title	Study Description	Number of Patients	Evidence Class	Conclusions
Kurihara (1998)[124]	Hemorrhage in pituitary adenoma: correlation of MR imaging with operative findings.	Patients with conventional MR imaging were retrospectively reviewed. The intensity of intratumoral cystic cavities using T2-weighted images were correlated with hemorrhage found at surgery as the gold standard.	113	Diagnostic / III	Twenty-nine of 52 hemorrhagic cysts demonstrated high/low signal (H/L) fluid-fluid levels on T2-weighted image (T2WI). In 19 of them, 2 components could be separately seen at operation: the supernatant high-intensity area represented xanthochromic fluid, and the dependent low-intensity area represented liquefied hematoma. The H/L fluid-fluid level was observed predominantly in hematomas on MR images obtained after longer intervals. In patients with repeated MR examination, follow-up MR imaging revealed additional hemorrhage or new formation of fluid-fluid levels. The preoperative MR images are well correlated to the operative findings in hemorrhagic pituitary macroadenomas. It proved that 52 of 54 cystic cavities had hemorrhagic components.
Lazaro (1994)[125]	Haemorrhagic pituitary tumours.	Clinical experience using TR/TE to assess pituitary lesions	12	Diagnostic / III	Intratumoral hemorrhage on MRI was characterized by high signal intensity on short TR/TE sequences and not different in hormone secreting versus NFPAs.

Author (Year)	Title	Study Description	Number of Patients	Evidence Class	Conclusions
Tosaka (2007)[126]	Assessment of hemorrhage in pituitary macroadenoma by T2*-weighted gradient-echo MR imaging.	Patients underwent both conventional MR and T2*-weighted MR imaging. Histology of surgical specimens was evaluated for hemorrhage. T2*-weighted characteristics were correlated with histologic assessments.	25	Diagnostic / III	T2*-weighted GE MR imaging detected various types of dark lesions, such as "rim," "mass," "spot," and "diffuse" and combinations, indicating clinical and subclinical intratumoral hemorrhage in 12 of the 25 patients. The presence of intratumoral dark lesions on T2*-weighted GE MR imaging correlated significantly with the hemorrhagic findings on T1- and T2-weighted MR imaging ($P < .02$ and $< .01$, respectively), and the surgical and histologic hemorrhagic findings ($P < .001$ and $< .001$, respectively). T2*-weighted GE MR imaging could detect intratumoral hemorrhage in pituitary adenomas as various dark appearances. T2* weighted GE MRI might be useful for the assessment of recent and old intratumoral hemorrhagic events in patients with pituitary macroadenomas.
Stadlbauer (2008)[89]	Proton magnetic resonance spectroscopy in pituitary macroadenomas: preliminary results.	Patients underwent proton MR (1H-MR) spectroscopy. Metabolite concentration of choline containing compounds was correlated to histological and surgical findings of hemorrhage as well as MIB-1 as a proliferative index.	16	Diagnostic / III	The study found a strong positive linear correlation between metabolite concentrations of Cho and the MIB-1 proliferative cell index ($R = 0.819$, $P < .001$). Eleven patients had a hemorrhagic adenoma and showed no assignable metabolite concentration of Cho, and the FWHM water was 13.4-24.4 Hz. In 10 patients, the size of the lesion was too small (<20 mm in 2 directions) for the acquisition of MR spectroscopy data. Quantitative 1H-MR spectroscopy provided important information on the proliferative potential and hemorrhaging of pituitary macroadenomas. These data may be useful for noninvasive structural monitoring of pituitary macroadenomas.

Table 10: Firmness of the Tumor Mass

Author (Year)	Title	Study Description	Number of Patients	Evidence Class	Conclusions
Yamamoto (2014)[53]	Tumor consistency of pituitary macroadenomas: predictive analysis on the basis of imaging features with contrast-enhanced 3D FIESTA at 3T.	Patients underwent both conventional MRI and contrast-enhanced 3D FIESTA sequences pre-operatively. Two neuroradiologists evaluated MR imaging findings, specifically those on the FIESTA scan. During surgery, neurosurgeons classified the tumors as soft or hard. Postoperatively, collagen content and residual tumor size was calculated. Fisher exact probability tests and independent sample *t* tests were used to compare predictions of MR imaging findings to intraoperative tumor consistency, tumor collagen content, and postoperative tumor size.	29	Diagnostic / III	Sensitivity and specificity were higher for contrast-enhanced FIESTA (1.00 and 0.88-0.92, respectively) than for contrast-enhanced T1WI (0.80 and 0.25-0.33, respectively) and T2WI (0.60 and 0.38-0.54, respectively). Compared with mosaic-type adenomas, solid-type adenomas tended to have a hard tumor consistency as well as a significantly higher collagen content and lower postoperative tumor size. Contrast-enhanced FIESTA can provide preoperative characterization of the consistency of pituitary adenomas.

Author (Year)	Title	Study Description	Number of Patients	Evidence Class	Conclusions
Suzuki (2007)[64]	Apparent diffusion coefficient of pituitary macroadenoma evaluated with line-scan diffusion-weighted imaging.	Patients prospectively underwent line-scan diffusion weighted imaging (LSDWI) and had ADC values calculated. These ADC values were correlated with the consistency recorded at surgery.	19	Diagnostic / II	A soft consistency was found at surgery in 13 patients (mean ADC: 0.84+/-0.1x10(-3) mm2/s); an intermediate consistency was observed in 6 patients (mean ADC: 0.81+/-0.16x10(-3) mm2/s). No tumors of hard consistency were found. There was no significant difference in ADC values between tumors of soft consistency compared with tumors of intermediate consistency (*P* = .37). A relationship between tumor consistency and the ADCs of soft and intermediate macroadenomas was not shown in this study using LSDWI.
Bahuleyan (2006)[128]	To assess the ability of MRI to predict consistency of pituitary macroadenomas.	Patients prospectively underwent MR imaging. MR imaging characteristics were compared to tumor consistency as reported by the surgeon.	80	Diagnostic / II	Of the firm tumors, 4 (33%) were homogeneously isointense, 1 (8%) was homogeneously hyperintense, and 7 (59%) were heterogeneous in appearance in T2-weighted images. The consistency of pituitary macroadenomas cannot be accurately predicted based on MRI signal intensities.

Author (Year)	Title	Study Description	Number of Patients	Evidence Class	Conclusions
Iuchi (1998)[129]	MRI prediction of fibrous pituitary adenomas.	MR imaging of patients with either firm or soft tumors, as identified at surgery, were retrospectively evaluated. Collagen content of surgical specimens and tumor densities on imaging was expressed as numerical data using NIH-image. The relationship between collagen content and imaging characteristics were compared.	26	Diagnostic / III	Signal intensities on T1-weighted images were not correlated with tumor consistency, whereas those on T2-weighted images were significantly correlated with the percentage of collagen content. Adenomas, showing lower signal intensities on T2-weighted images, contained more collagen. On enhanced images, homogeneously enhanced adenomas tended to include more collagen, even though the grade of enhancement effect showed only weak correlation with the tumor hardness. Adenomas may be firm and fibrous if they show low signal intensities on T2-weighted images and homogeneous enhancement.
Kanou (2002)[130]	Clinical implications of dynamic MRI for pituitary adenomas: clinical and histologic analysis.	Patients underwent both conventional MR and dynamic MR imaging. Enhancement patterns and factors such as hormone status, tumor size, vascularity, arterial involvement, and tumor texture were compared in 2 image modalities.	67	Diagnostic / III	Adenomas inclined to have late enhancement patterns were relatively small compared to those with early patterns. Tumors with very early enhancement patterns were significantly more fibrous than those with the other 3 patterns. The factors that contribute to sequential enhancement patterns remain unclear. The dynamic sequential pattern may provide useful information about the texture of the tumor.

Author (Year)	Title	Study Description	Number of Patients	Evidence Class	Conclusions
Mahmoud (2011)[63]	Role of PROPELLER diffusion-weighted imaging and apparent diffusion coefficient in the evaluation of pituitary adenomas.	Patients who underwent conventional MR and periodically rotated overlapping parallel lines with enhanced reconstruction (PROPELLER) DWI were retrospectively analyzed. Mean, max, and min values from the PROPELLER DWI images were calculated. Intraoperative tumor consistency was recorded by neurosurgeons. ADC values were compared to tumor consistency experienced intraoperatively and percent collagen content.	19	Diagnostic / III	Tumor consistency was strongly associated with the percent collagen content. However, neither the tumor consistency nor the percent collagen content was correlated with MRI findings or ADC values. The SI of growth hormone-producing adenomas on T2-WI was lower than of the other pituitary adenomas studied ($P <$ .01); no other significant difference was found in the ADC or on conventional MRI between pituitary adenomas with different secretory functions. The MIB-1 LI of pituitary adenomas was not correlated with their appearance on conventional MRI or their ADC values. Unlike other studies, this study found tumor consistency was not correlated with ADC findings.

Author (Year)	Title	Study Description	Number of Patients	Evidence Class	Conclusions
Pierallini (2006)[131]	Pituitary macroadenomas: preoperative evaluation of consistency with diffusion-weighted MR imaging—initial experience.	Patients underwent both conventional MR and diffusion-weighted imaging. ADC was calculated and compared to the consistency of tumor evaluated at surgery as well as histologic characteristics such as percentage of collagen content.	22	Diagnostic / III	The mean value of ADC in the soft group was (0.663 +/- 0.109) x 10(-3) mm(2)/sec; in the intermediate group, (0.842 +/- 0.081) x 10(-3) mm(2)/sec; and in the hard group, (1.363 +/- 0.259) x 10(-3) mm(2)/sec. Statistical analysis revealed a significant correlation between tumor consistency and ADC values, DW image SI ratios, T2-weighted image SI ratios, and percentage of collagen content ($P < .001$, analysis of variance). Findings in this study suggest that DW MR images with ADC maps can provide information about the consistency of macroadenomas.

Author (Year)	Title	Study Description	Number of Patients	Evidence Class	Conclusions
Boxerman (2010)[132]	Preoperative MRI evaluation of pituitary macroadenoma: imaging features predictive of successful transsphenoidal surgery.	Patients with chiasm-compressing tumors who underwent conventional MR and DWI imaging were retrospectively evaluated. MR images were used to identify nonsolid and solid tumors by 2 neuroradiologists. Apparent diffusion coefficient values, T2-weighted signal intensity normalized to pons intensity were also calculated. Postoperative scans were evaluated for chiastmatic decompression and mean change in tumor height. Chiastmatic decompression defined surgical success. A neuropathologist assessed reticulin content in tumor samples. Each of these parameters was correlated with preoperative imaging findings using chi-square, Fisher exact, and *t* tests.	28	Diagnostic / III	The ratios of tumor to brainstem ADC in the 9 successfully resected solid tumors were higher than in the 8 cases of failed treatment (P = .008). All 6 solid tumors with enhanced diffusivity (ratio of tumor to brainstem ADC > 1.1) were successfully managed with transsphenoidal hypophysectomy, compared with 3 of 11 with an ADC ratio less than 1.1 (P = .009). Tumors with nonsolid features or an ADC ratio greater than 1.1 were highly resectable (P < .001; sensitivity, 0.84; specificity, 0.89). ADC ratios in reticulin-poor solid tumors were higher than those in reticulin-rich tumors (P = 0.024). Macrocystic and macrohemorrhagic adenomas and solid tumors with enhanced diffusivity determined with ADH are more likely to be successfully managed with transsphenoidal hypophysectomy. Transsphenoidal hypophysectomy of solid, enhancing tumors with restricted diffusion is more likely to fail. This may help with case selection for transsphenoidal versus transcranial approaches.

Table 11: Pituitary Anatomy

Author (Year)	Title	Study Description	Number of Patients	Evidence Class	Conclusions
Sumida (1994)[133]	MRI of pituitary adenomas: the position of the normal pituitary gland.	Study characterizing the MRI appearance of the normal pituitary anatomy relative to pituitary lesions.	20	Diagnostic / III	The high intensity of the posterior lobe could be differentiated using T1-weighted sagittal imaging in 13 patients (52%). The normal pituitary gland, which enhanced more strongly than tumor, could be differentiated using Gd-DTPA-enhanced MRI on the sagittal images in 22 cases (88%) and on the coronal image in 17 (68%). In 7 patients, the normal pituitary gland surrounded the tumor; it was displaced superiorly in 14 cases and superioposteriorly in 2 but in no case was it displaced anteriorly or downwards. One preoperative radiologic characteristic that can help with the differential diagnosis of sellar lesions can come from the displacement of the normal pituitary gland.
Sumida (1994)[134]	Displacement of the normal pituitary gland by sellar and juxtasellar tumours: surgical-MRI correlation and use in differential diagnosis.	Study characterizing the displacement of normal pituitary gland by pituitary adenomas.	22	Diagnostic / III	The direction of displacement of the normal pituitary gland correlated well with tumor type, so that its position proved helpful in the differential diagnosis. The normal gland was typically displaced superiorly by pituitary adenomas, inferiorly by craniopharyngiomas, and anteriorly by germinomas. One preoperative radiologic characteristic that can help with the differential diagnosis of sellar lesions can come from the displacement of the normal pituitary gland.

Author (Year)	Title	Study Description	Number of Patients	Evidence Class	Conclusions
Fujisawa (2002)[135]	Bright pituitary stalk on MR T1-weighted image: damming up phenomenon of the neurosecretory granules.	Patients with and without pituitary adenomas underwent conventional MR imaging. Using T1-weighted images, the pituitary stalk was analyzed and correlated to presence of central diabetes insipidus.	13	Diagnostic / III	The normal pituitary stalk appears as a low-intermediate intensity signal on sagittal and coronal T1WIs with 3 mm-slice thickness. The pituitary stalk appeared as a bright signal in 20 patients; 13 with pituitary adenoma. No patients suffered from symptoms of central DI when the bright pituitary stalk appeared. There is a significance of the bright pituitary stalk that may suggest functional integrity of the endocrine system and may suggest endocrine function in images.
Smith (1994)[136]	Magnetic resonance imaging measurements of pituitary stalk compression and deviation in patients with nonprolactin-secreting intrasellar and parasellar tumors: lack of correlation with serum prolactin levels.	Conventional MR imaging of patients with NFPAs and secretory adenomas were reviewed. Images were assessed for tumor size, angular deviation of the pituitary stalk, and compression of the pituitary stalk. These imaging findings were compared to prolactin levels of the different tumors.	15	Diagnostic / III	There was no significant correlation of PRL level and the degree of pituitary stalk compression, stalk deviation, or tumor size. PRL levels were found to be markedly elevated in some patients with a tumor causing little distortion of the pituitary stalk. Conversely, PRL levels were often normal despite evidence of massive distortion of the stalk. Magnetic resonance imaging evidence of pituitary stalk distortion cannot be used to determine the diagnosis of prolactinoma versus pseudoprolactinoma in most cases.

Author (Year)	Title	Study Description	Number of Patients	Evidence Class	Conclusions
Bonneville (2002)[137]	Preoperative location of the pituitary bright spot in patients with pituitary macroadenomas.	Patients with nonenhanced spin-echo T1-weighted MR images were retrospectively reviewed to identify the location of the high-intensity signal posterior pituitary lobe and correlated to endocrine outcomes.	54	Diagnostic / III	The bright spot corresponding to ADH storage was identified in 44 (81%) patients. Two groups of patients were defined by the height of the macroadenoma: Group A patients (n = 27) had pituitary macroadenomas less than 20 mm in height, and group B (n = 27) had macroadenomas 20 mm or larger. In group A, the bright spot was identified in 25 patients (93%); it was located in the sella in 24 of these cases (96%). In group B, the bright spot was identified in 19 patients (70%); it was in an ectopic location in 14 of these cases (74%). MR imaging can be used to depict the pituitary bright spot in most patients with pituitary macroadenomas before surgery. The bright spot is usually identified at its expected location within the sella in patients with pituitary macroadenomas less than 20 mm in height, whereas an ectopic location is common when pituitary macroadenomas are larger than 20 mm.

Author (Year)	Title	Study Description	Number of Patients	Evidence Class	Conclusions
Takahashi (2005)[138]	Ectopic posterior pituitary high signal in preoperative and postoperative macroadenomas: dynamic MR imaging.	Patients underwent conventional MR imaging preoperatively. Enhancement of the posterior pituitary high signal on T1-weighted MR images were assessed. The presence and location of posterior pituitary high signal was correlated with tumor volume.	111	Diagnostic / III	Preoperatively, PPHS was seen only in the normal location in 29 patients (Group A: 26.1%). High signal was detected only in an ectopic location in 58 patients, and early enhancement of this ectopic high signal was confirmed by dynamic MR imaging in 56 patients (Group B: 50.5%). No PPHS was observed in 24 patients (Group C: 21.6%). Adenoma volume was significantly greater for Group B than for Group A (P < .001). Among the Group B patients who underwent MR imaging postoperatively (n = 31), the location of PPHS was not changed, except for 2 patients in whom PPHS was absent. Greater volume of adenoma is associated with a higher incidence of ectopic PPHS, and the ectopic change is irreversible.

Author (Year)	Title	Study Description	Number of Patients	Evidence Class	Conclusions
Saeki (Feb 2003)[139]	Posterior pituitary bright spot in large adenomas: MR assessment of its disappearance or relocation along the stalk.	Patients with conventional MR imaging were classified into posterior pituitary bright spot visible and nonvisible groups using T1-weighted MR images. Tumor shapes were classified into hourglass or barrel types. These imaging findings were compared to presence of diabetes insipidus.	69	Diagnostic / III	Posterior pituitary bright spot most commonly occurred at the distal pituitary stalk immediately above the diaphragm in 48 patients with hourglass-type adenoma. In the remaining 7 patients with barrel-type adenoma, PPBS occurred in the sella or in varying sites along the pituitary stalk. Postoperatively, 2 patients, whose PPBS became nonvisible, developed persistent diabetes insipidus. The PPBS-nonvisible group included 14 (20%) patients. Five had hourglass-type and 9 had barrel-type adenoma. Occurrence of the barrel type was marked. In these patients, 4 developed postoperative permanent diabetes insipidus. PPBS was more commonly nonvisible in the barrel-type adenoma and is associated with postoperative DI.
Eda (2002)[140]	Demonstration of the optic pathway in large pituitary adenoma on heavily T2 weighted MR images.	Patients underwent T2-weighted reversed MR imaging. The relation of the pituitary adenoma to optic pathway and the appearance of the optic chiasm was identified. These imaging findings were correlated to the degree of visual field deficits.	28	Diagnostic / III	The optic chiasm was located anterior in 4 cases, superior in 22, and posterior in 2 in relation to the adenoma. Detectability of each optic component was higher on T2R images than on conventional T1-weighted images. This preoperative MRI information makes it possible to visualize directly the optic pathway even in huge adenomas and is useful in predicting surgical anatomy and selecting a proper surgical approach.

Author (Year)	Title	Study Description	Number of Patients	Evidence Class	Conclusions
Sumida (1998)[141]	Demonstration of the optic pathway in sellar/juxtasellar tumours with visual disturbance on MR imaging.	Patients with sellar/juxtasellar tumors and visual field defects prospectively underwent spoiled gradient recalled acquisition in steady state or conventional MR imaging. Visualization of the optic pathway was compared using the 2 modalities.	108	Diagnostic / III	The rates for visualization of the optic nerves, chiasms, and tracts were 50%, 77.8%, and 89.8%, respectively. In contrast, on SPGR coronal image the rates were 80.6%, 96.3%, and 92.6% respectively. The rate of visualization of optic pathway structures on SPGR imaging (without enhancement) is greater than that on CSE T1-weighted imaging. This may be important in preoperative for surgical planning for lesions around the sella turcica.
Carrim (2007)[142]	Predicting impairment of central vision from dimensions of the optic chiasm in patients with pituitary adenoma.	Patients with MR imaging and Goldman perimetry charts were evaluated. Area of the chiasm, central height of the chiasm, and perpendicular height of the tumor were correlated with visual field impairments.	19	Diagnostic / III	There was a strong, statistically significant linear correlation between H (chiasm) and bitemporal (Pearson's coefficient r = -0.69, *P* = .001), binocular (r = -0.63, *P* = .004), and binasal (r = -0.52, *P* = .01) central field loss. A similar relationship was observed between H (tumor) and bitemporal (r = 0.55, *P* = 0.015) and binocular (r = 0.46, *P* = .05) central field loss. Height of the chiasm and height of the tumor on MRI preoperatively can be used to predict extent of central visual impairment.

Author (Year)	Title	Study Description	Number of Patients	Evidence Class	Conclusions
Tokumaru (2006)[143]	Optic nerve hyperintensity on T2-weighted images among patients with pituitary macroadenoma : correlation with visual impairment.	Patients underwent conventional MR imaging. T2-weighted images were used to evaluate optic nerves in terms of: signal intensity and degree of optic chiasm compression. The imaging characteristics were compared to visual field disturbances.	27	Diagnostic / II	Signal intensity abnormality of the optic nerve was seen at the site of compression and in the ventral side of the tumor. These patients did not demonstrate signal intensity abnormality posterior to the tumor. Presence of such signal intensity abnormalities was correlated with the degree of optic chiasmal compression and with VA disturbance. Recovery of VA after treatment was correlated with disease duration. Hyperintensity of the optic nerves ventral to the pituitary macroadenoma was associated with VA impairment. Recovery of VA after treatment was correlated with disease duration. MR imaging of the optic nerves can provide valuable information for identification of visual impairment and prognosis.
Saeki (2003)[144]	MR imaging study of edema-like change along the optic tract in patients with pituitary region tumors.	Patients with pituitary adenomas touching or compressing the optic pathway underwent T2-weighted MR imaging. Images were assessed for edema-like change along the optic tract and correlated to optic chiasm compression.	25	Diagnostic / III	After therapeutic decompression of the optic pathway, the edema-like change disappeared and large Virchow-Robin spaces, present under normal conditions, became visible along the optic tract. Edema-like change occurs in association with pituitary region tumors other than craniopharyngiomas.

APPENDIX A

Search Strategies

pubmed

(microadenoma* OR adenoma* OR macroadenoma* OR incidentaloma* OR chromophobe* OR transsphenoidal*[Title/Abstract]) AND (pituitary OR hypophyse* OR sellar OR transsphenoidal[Title/Abstract]) AND (imag* OR MRI OR CT OR spectroscopy* OR proton OR PET* OR SPECT* OR stereota* OR navigation*[Title/Abstract])

COCHRANE

1. MeSH descriptor Pituitary Neoplasms
2. MeSH descriptor Adenoma
3. 1 and 2
4. ((pituitary OR hypophyse* OR sellar) NEAR/4 (microadenoma* OR adenoma* OR macroadenoma* OR incidentaloma* or chromophobe*)):ti,ab,kw
5. 3 or 4 and (asymptomatic* OR nonfunction* OR non-function* OR nonsecret* OR non-secret* OR inactive OR null OR inert OR silent)